Tellus (1993), 45A, 221–246
Printed in Belgium – all rights reserved

TELLUS
ISSN 0280–6495

A simple time-dependent coupled ice-ocean model with application to the Greenland-Norwegian Sea

By M. S. DARBY* and A. J. WILLMOTT, *Department of Mathematics, University of Exeter, North Park Road, Exeter, EX4 4QE, England*

(Manuscript received 2 December 1991; in final form 18 January 1993)

ABSTRACT

A time-dependent single active layer reduced gravity thermodynamic upper ocean model is coupled to a thermodynamic dynamic sea-ice model and is used to investigate sea-ice cover in the Greenland-Norwegian Sea on the seasonal to interannual time scales. The model is driven by prescribed wind stress, air temperature and salinity and temperature distributions across the open zonal boundaries located at 60°N and 80°N. Two spin-up experiments which employ steady forcing fields, but differ in the magnitude of the shear stress between air and ice, demonstrate that regions of high salinity can become convectively unstable leading to vertical mixing and hence reduced ice cover. In particular, increasing the magnitude of the air-ice shear stress leads to an enhanced stress acting on the surface of the ocean, and this in turn leads to a northwards extension of the region which is preconditioned for convective overturning. When the model is forced by time-dependent air temperatures, the predicted seasonal behaviour of the 10%, 50% and 90% ice concentration contours agrees well with observations. The increased sea-ice cover associated with the Great Salinity Anomaly during the late 1960s is also successfully simulated by the model.

1. Introduction

Ice affects the transfer of heat and momentum between atmosphere and ocean and therefore must be an important component of any climate model. High-latitude navigation, strategic operations and resource development also require accurate information regarding ice cover and ice thickness. These requirements have motivated the development of various coupled ice-ocean models.

Existing coupled ice-ocean models fall into various categories:

(i) One-dimensional coupled ice-ocean models which usually use the Semtner (1976) thermodynamic ice model coupled to a one-dimensional mixed layer model. This type of model is usually applied on the climatic time-scale and may be used to simulate Arctic ice mass variations (e.g., Häkkinen and Mellor, 1990; Riedlinger and Warn-Varnas, 1990).

(ii) Mesoscale wind-driven models of the marginal ice zone which employ simplified ice and ocean dynamics, often neglect ice thermodynamics and are applied on the relatively short time-scale of a few days (e.g., Häkkinen, 1986; Ikeda, 1991).

(iii) Three-dimensional large scale numerical coupled ice-ocean models. These frequently employ the Hibler (1979) thermodynamic-dynamic ice model coupled to a sophisticated three dimensional ocean general circulation model (e.g., Hibler and Bryan, 1984, 1987; Fleming and Semtner, 1991).

Of the above models, only those in the last category include a realistic spatially varying ocean, known to be essential for accurate determination of ice cover (see Fleming and Semtner, 1991). However, models in the third category require large computer resources thus limiting their use in

* Corresponding author.

climate studies. The large computer requirements stem from the use of a sophisticated three-dimensional ocean model and the restrictive time-step associated with the Hibler (1979) ice-dynamics code. Clearly, for climate studies a coupled ice-ocean model is required which retains spatial variability but uses a simple ocean model and a more efficient ice-dynamics model.

Willmott and Mysak (1989) (henceforth referred to as WM) present a steady state coupled ice-ocean model which consists of a simple thermodynamic ice model coupled to a thermodynamic single active layer reduced gravity model. Ice dynamics is neglected in the WM study. The WM model is applied to the Greenland-Norwegian sea region, forced with climatological wind stress curl, atmospheric temperature and southern boundary inflow temperature and found to yield a realistic upper ocean flow, temperature field and ice-edge position. Wood and Mysak (1989) extend the WM model to include horizontal diffusion of heat and momentum and a representation of the East Greenland Current (henceforth referred to as EGC), but they retain the steady-state assumption. The new feature obtained in the Wood and Mysak (1989) study is that where a closed gyre occurs and diffusion of heat is small the ice-edge meanders and the ice depths acquire a local maximum. Columns of fluid in a recirculating gyre cool until the heat lost through the ice to the atmosphere is balanced by the diffusion of heat from the surrounding ocean.

In this study, we extend the WM model to include time-dependence, active salinity, horizontal diffusion of heat and salt, upwelling, a simple convection parameterization, ice dynamics, frazil ice production and a prognostic ice concentration equation. All of these realistic processes play a vital role in the results presented. The governing equations are scaled for seasonal to interannual time scales and thus the resulting model has potential applications in climate change studies. The simplicity of the model (relative to those in category (iii) above) enables complex coupled ice-ocean mechanisms to be easily interpreted. We propose that this type of model may pinpoint processes which merit further study using a fully three-dimensional model.

The model is again applied to the Greenland-Norwegian sea region. However, it should be noted that the model formulation is general, and could be applied to many other polar regions (e.g., the Labrador and Weddell Seas). The primary objective of this paper is to present the model, and show that the model physics produces a rich variety of behaviour that sheds light on fundamental coupled ice-ocean processes. Application of the model to the Greenland-Norwegian sea allows a comparison to be made between the final steady spin-up states with the steady state solutions in the WM study. Simulating the ice-ocean interactions of the Greenland-Norwegian Sea also provides a testing application of the model because it requires the development of robust inflow/outflow boundary conditions for sea ice. Ice enters the domain through the northern boundary and exits through the southern boundary. Models for the entire Arctic and Antarctic only require robust outflow boundary conditions for sea-ice.

Results are presented for two spin-up experiments from rest, which differ in the magnitude of the shear stress between the atmosphere and ice. Under ice ocean temperatures are usually close to the freezing point of sea water (taken to be $-1.8\,^{\circ}C$) and are much cooler than the deep abyssal water. Under most circumstances vertical stratification is retained because the active layer has lower salinity than the abyssal region. In high salinity regions, vertical mixing may occur, leading to upwelling of warm abyssal water into the active layer and hence contribute towards melting of overlying ice. In this study, we show that the region preconditioned for deep convection occurs near the centre of the Greenland Sea cyclonic gyre (a mechanism also discussed by Gascard (1990)). The strength of the gyre and the location of the gyre centre is controlled by the magnitude of the shear stress at the surface of the ocean; enhancing air-ice shear stress leads to enhanced ice-water shear stress and a subsequent poleward migration of the region preconditioned for deep convection.

WM specify a zero net meridional mass transport condition which in combination with realistic wind stress curl leads to an unrealistic northerly flowing western boundary current in the northwest corner of the domain. By specifying a net southwards transport of 13 Sv combined with a modified wind stress, the circulation is shown to be considerably more realistic. In particular, an equatorward flowing EGC is obtained at all latitudes within the domain.

Experiments employing annual time-dependent

atmospheric temperatures lead to realistic (when compared with the observed seasonal ice concentration contour behaviour, documented in the atlas of Manak and Mysak (1987)) evolution of the ice concentration contours. In spring the 10%, 50% and 90% concentration contours are closely spaced whereas in autumn they all retreat polewards with a large spacing between the 50% and 90% contours. Winter ice-edge positions are found to be most sensitive to the presence of convectively unstable regions.

In the 1960s, a fresh water anomaly, referred to as the great salinity anomaly (henceforth referred to as GSA), propagated cyclonically around the Arctic seas. Mysak et al. (1990) and Marsden et al. (1991) demonstrate a correlation between the passing of this anomalous fresh water cell and periods of large ice extent. Furthermore, Mysak et al. (1990) propose that the GSA may be a component in an interdecadal Arctic climate cycle involving atmosphere-ocean-cryosphere feedbacks. This idea is pursued further by Darby and Mysak (1992) using a Boolean delay equation model for the proposed interdecadal Arctic climate cycle. Using the coupled ice-ocean model, we also successfully simulate the sensitivity of sea-ice to the GSA event. A period of anomalous fresh inflow water at the northern boundary (which simulates the GSA) is found to suppress overturning and hence lead to increased ice cover.

The plan of the paper is as follows. In Section 2 we describe the ocean model. In Section 3, the thermodynamic dynamic ice model equations are discussed. In Section 4, the equations are non-dimensionalized and the numerical solution method described. Results from the coupled ice-ocean model are presented in Section 5. Conclusions and future directions for research are given in Section 6.

2. The ocean model

The Greenland Sea between 60° N and 80° N is represented by a meridionally aligned channel on a β-plane. The ocean component of the coupled ice-ocean model consists of a single active layer thermodynamic reduced gravity model similar to that described by Willmott and Darby (1990). The ocean surface may be covered by ice of depth $d(x, y, t)$ and concentration $A(x, y, t)$. The depth-integrated equations which govern conservation of momentum, mass, heat and salt in the layer are:

$$\frac{\partial(hu)}{\partial t}+\nabla\cdot(h\boldsymbol{u}u)-fvh=-\frac{\partial P}{\partial x}-gh\,\Delta^{*}A\frac{\partial d}{\partial x}+\frac{1}{\rho_0}[(1-A)\tau^{x}_{wa}+A\tau^{x}_{wi}]-ruh, \tag{2.1}$$

$$\frac{\partial(hv)}{\partial t}+\nabla\cdot(h\boldsymbol{v}u)+fuh=-\frac{\partial P}{\partial y}-gh\,\Delta^{*}A\frac{\partial d}{\partial y}+\frac{1}{\rho_0}[(1-A)\tau^{y}_{wa}+A\tau^{y}_{wi}]-rvh, \tag{2.2}$$

$$\frac{\partial h}{\partial t}+\nabla\cdot(\boldsymbol{u}h)+w-w_e=0, \tag{2.3}$$

$$\frac{\partial(hT)}{\partial t}+\nabla\cdot(\boldsymbol{u}hT)=-(1-A)\frac{Q_{wa}}{\rho_0 c_p}-A\frac{Q_{wi}}{\rho_0 c_p}-Q_{FR}-wT_B+w_eT_0+A_T\nabla\cdot(h\nabla T)+\frac{\rho_i d}{\rho_0 c_p}S_A\left\{L_w+c_i\left(\frac{T_B-T_S}{2}\right)\right\}, \tag{2.4}$$

$$\frac{\partial(hS)}{\partial t}+\nabla\cdot(\boldsymbol{u}hS)=-wS_i+w_eS_0+A_S\nabla\cdot(h\nabla S), \tag{2.5}$$

where

$$P=\frac{1}{2}g\,\Delta^{*}h^{2},\qquad \Delta^{*}=\frac{\rho_0-\rho}{\rho_0}. \tag{2.6}$$

The set of equations (2.1)–(2.5) are referred to a right-handed Cartesian coordinate system in which x is directed eastward, y northward and z vertically upwards. Gravitational acceleration is denoted by g and $f=f_0+\beta y$ denotes the Coriolis parameter. The motionless lower layer has constant temperature, T_0, salinity, S_0, and density, ρ_0. In the upper layer of depth h, the depth independent velocity $\boldsymbol{u}=(u, v)$. The components of wind stress acting on the ocean surface are $(\tau^{x}_{wa}, \tau^{y}_{wa})$ and are defined by

$$\boldsymbol{\tau}_{wa}=\rho_a c_D\,|\boldsymbol{u}_a|\,\boldsymbol{u}_a,$$

where ρ_a denotes the air density, c_D is the water-air drag coefficient and $\boldsymbol{u}_a$ is the air velocity. The com-

ponents of shear stress acting at the ice-ocean interface are $(\tau^x_{wi}, \tau^y_{wi})$ and are defined by

$$\boldsymbol{\tau}_{wi} = \rho_i c_{wi} |\boldsymbol{u}_i - \boldsymbol{u}| (\boldsymbol{u}_i - \boldsymbol{u}),$$

where ρ_i denotes the ice density, c_{wi} is the water-ice drag coefficient and $\boldsymbol{u}_i = (u_i, v_i)$ denotes the ice velocity. The terms $rh(u, v)$ in (2.1) and (2.2) represent linear bottom drag and lead to a simple Stommel-type western boundary current.

Ice concentration is denoted by A so that in an infinitesimal rectangular region of area $\delta x\, \delta y$, an area $A\, \delta x\, \delta y$ is ice covered. The upper layer density $\rho(x, y, t)$, temperature $T(x, y, t)$ and salinity $S(x, y, t)$ are related via a linear equation of state of the form

$$\rho = \rho_0[1 - \alpha(T - T_0) + \gamma(S - S_0)],$$

where α and γ are the thermal and salinity expansion coefficients respectively.

Following Røed (1984), the net heat fluxes through the water-air interface (Q_{wa}), water-ice interface (Q_{wi}) and ice-air interface (Q_{ia}) are parameterized by

$$Q_{wa} = -\kappa_{wa}(T_A - T), \qquad Q_{wi} = -\kappa_{wi}(T_B - T),$$
$$Q_{ia} = -\kappa_{ia}(T_A - T_S), \tag{2.7}$$

where T_B is the temperature at the base of the ice (taken to be a constant value of $-1.8\,^\circ$C), T_A is the atmospheric temperature at the sea surface and T_S is the surface ice temperature. κ_{wa}, κ_{wi} and κ_{ia} are appropriate heat exchange coefficients. In (2.4) c_p is the specific heat capacity of sea water. If $T < T_B$ occurs (this does not occur in the solutions presented in Section 5 but for generality the equations are derived to allow for this possibility), frazil ice is considered to crystallize out of the water column and accrete on the ice base. This process is parameterized by the heat flux term Q_{FR} in eq. (2.4), where

$$Q_{FR} = H(T_B - T)\left[\frac{h(T - T_B)}{2\Delta t} - (1 - A)\frac{Q_{wa}}{\rho_0 c_p}\right], \tag{2.8}$$

is chosen to approximately return active layer temperature to T_B over one time-step, Δt, of the numerical model. In (2.8), H denotes the Heaviside function.

In the absence of entrainment of abyssal water into the active layer we find that, for realistic values of $(\tau^x_{wa}, \tau^y_{wa})$, T_A and Δ^* the active layer depth tends to be rather deep when compared with typical mixed layer depths. The final spun-up steady-state of such a model produces realistic active layer temperatures and currents, but the response to time-dependent forcing occurs only on the interannual time scale rendering the model inappropriate for important seasonal time scale problems (see the Willmott and Darby (1990) study for a discussion of this problem). To overcome this problem, whilst retaining the model's simplicity, we include a vertical entrainment velocity, w_e, across the base of the active layer, which appears in (2.3) to (2.5). There are many possible choices for w_e; sophisticated mixed layer models (e.g., de Szoeke, 1980) parameterize w_e as a function of the wind stress, surface heat flux, Δ^* and various empirical constants. We include w_e to prevent the active layer depth shoaling to zero during the spin-up of the model and assume, for simplicity, that $w_e = A_v/h$ where A_v is a vertical diffusion coefficient taken to be the same for both heat and salt. It can be considered that this term parameterizes the effect of vertical diffusion of heat and salinity across the mixed layer base. To derive the form of these terms, the vertical diffusion terms $(A_v T_z)_z$ and $(A_v S_z)_z$ are included in the temperature and salinity equations prior to vertically integrating them over the active layer. In a $2\frac{1}{2}$-layer model, McCreary and Yu (1992) employ a simplified expression for entrainment velocity which, in common with the form of w_e used here, results in entrainment increasing as upper layer depth decreases.

It is believed that deep convection is an important process in the Greenland Sea (see Clarke et al. (1990), for example). We attempt to parameterize the effect of deep convection on active layer temperature, and hence ice cover, by vertically mixing the water column where regions of negative P (which correspond to convectively unstable regions) occur. The details of this procedure are described in Subsection 4.2.

Notice also that changes in ice depth, d, and ice concentration, A, lead to a vertical velocity, w, at the top of the active layer given by

$$w = \frac{\rho_i}{\rho_0}(AS_d + dS_A), \tag{2.9}$$

where S_d and S_A denote the thermodynamic component of $\partial d/\partial t$ and $\partial A/\partial t$, respectively. Ice depth and ice concentration changes can also occur via ice dynamics (e.g., convergence of ice leads to an ice depth increase and possibly "ridging") and we are careful to distinguish between this mechanism and changes produced by thermodynamics. S_d and S_A are defined in Section 3.

In (2.4) and (2.5), A_T and A_S are horizontal diffusion coefficients for heat and salt respectively. Note the form of the diffusion terms is different to that given in Wood and Mysak (1989). Application of the divergence theorem to the region under consideration shows that the form of the diffusion terms given here globally conserves heat and salt, unlike that given by Wood and Mysak (1989) (which can lead to spurious sources and sinks of heat and salt).

The heat required to change A is supplied from the water column below the ice. The final term in (2.4) allows for a heat gain (loss) by the water column below ice when A is increasing (decreasing). L_w denotes the latent heat of fusion of sea water and c_i denotes the specific heat capacity of sea ice. The ice is assumed to have constant salinity S_i.

To summarize, eqs. (2.1)–(2.5) are 5 equations for the 9 unknowns u, v, h, T, S, u_i, v_i, d and A. To close the system we require governing equations for u_i, v_i, d and A.

3. The ice model

The equations which govern conservation of ice momentum, ice mass and ice concentration are

$$\frac{\partial(\mathrm{d}u_i)}{\partial t} + \nabla\cdot(\mathrm{d}u_i\boldsymbol{u}_i) - fv_i d = \frac{1}{\rho_i}\left(\tau^x_{ia} - \tau^x_{wi} - S_m\frac{\partial(\mathrm{d}A)}{\partial x}\right), \tag{3.1}$$

$$\frac{\partial(\mathrm{d}v_i)}{\partial t} + \nabla\cdot(dv_i\boldsymbol{u}_i) + fu_i d = \frac{1}{\rho_i}\left(\tau^y_{ia} - \tau^y_{wi} - S_m\frac{\partial(\mathrm{d}A)}{\partial y}\right), \tag{3.2}$$

$$\frac{\partial(Ad)}{\partial t} + \nabla\cdot(A\,\mathrm{d}\boldsymbol{u}_i) = AS_d + dS_A + A_d\nabla\cdot(A\nabla d), \tag{3.3}$$

$$\frac{\partial A}{\partial t} + \nabla\cdot(A\boldsymbol{u}_i) = S_A + L_A + A_A\nabla^2 A, \tag{3.4}$$

where the air-ice shear stress

$$\tau_{ia} = \rho_a c_{ia}\,|\boldsymbol{u}_a|\,\boldsymbol{u}_a,$$

and c_{ia} denotes the ice-air drag coefficient. The final term in (3.1) and (3.2) enables the ice velocity field to satisfy no normal flow at the rigid boundaries and is of a similar form to that employed by Semtner (1987). In this study S_m is simply taken to be a constant, whereas Semtner (1987) parameterizes the resistance of ice to compression via a dependence of S_m on the divergence of the ice velocity field. At points where the flow is divergent, Semtner (1987) sets S_m to zero on the grounds that ice interactions are negligible in such regions. Adopting the Semtner (1987) formulation for S_m in this model led to a non-zero "pressure gradient term" at points distributed "patchily" in space and time and this promoted noisy fields for d and A. By taking S_m as constant, the solutions are numerically stable. Further, constant S_m still leads to a model which correctly exhibits the qualitative behaviour of sea–ice to compression; the momentum balances (3.1) and (3.2) reduce to free-drift except in regions of large ice depth gradients which tend to be regions of ice convergence.

This simplification is found to assist the stability of the numerical solution procedure and is justified since S_m is chosen such that the momentum balance is predominantly free drift except in regions of large ice depth gradients which tend to be regions of ice convergence.

The term L_A in (3.4) limits ice concentration increases such that $A \leqslant A_{max}$. Choosing $A_{max} < 1$ ensures there is always a small fraction of open water. The diffusion terms in (3.3) and (3.4) are found to be necessary for numerical stability and the values of A_d and A_A are chosen so that the terms are relatively small (see Appendix B for parameter values).

The ideas used to derive an expression for ice-depth presented by WM are now extended to

derive an expression for S_d. We make the following assumptions:

(a) ice only forms/melts at the ice base;
(b) the ice temperature at the base, T_B, is constant;
(c) in one dimensional ice models, it is usual to assume (Semtner, 1976) that ice temperature is determined by the heat equation

$$\frac{\partial T_i}{\partial t} = \frac{\kappa_i}{\rho_i c_i} \frac{\partial^2 T_i}{\partial z^2}, \tag{3.5}$$

where κ_i and T_i are the thermal conductivity of ice and interior ice temperature, respectively; it is clear from (3.5) that adjustment towards a linear temperature profile within ice of thickness d occurs on the time scale $(\rho_i c_i d^2)/\kappa_i$, which is about 5.5 days when $d = 1$ m; however, the model time-scale is annual to interannual so it is a reasonable approximation to assume that, for ice depths of a few metres, the temperature decreases linearly from T_B at the base to T_S at the surface;
(d) the ice salinity, S_i, is constant;
(e) the Haney-type heat fluxes (2.7) used by WM are valid;
(f) horizontal diffusion of heat in the ice is negligible; this assumption is supported by the fact that the aspect ratio for sea ice (defined as, typical ice depth/typical horizontal length scale of the ice) is a small parameter.

The interior vertical heat flux, Q_i, within the ice is given by

$$Q_i = -\kappa_i \frac{\partial T_i}{\partial z}.$$

Assumption (a) implies that $Q_i = Q_{ia}$ or

$$-\kappa_{ia}(T_A - T_S) = -\kappa_i \frac{(T_S - T_B)}{d}, \tag{3.6}$$

which may be rewritten as

$$T_S = \frac{\kappa_i T_B + \kappa_{ia} T_A d}{\kappa_{ia} d + \kappa_i}. \tag{3.7}$$

If we now consider the heat balance for an ice column and employ (3.3), (3.4) and (3.7) the following expression for S_d is obtained:

$$S_d = \frac{\left(\begin{array}{l} \dfrac{Q_{FR}}{A} + Q_{wi} - Q_{ia} - c_i \rho_i d \Big[d\hat{\kappa} \dfrac{\partial T_A}{\partial t} \\ \quad + \boldsymbol{u}_i \cdot \nabla \left(\dfrac{T_S + T_B}{2} \right) + \hat{\kappa}(T_A - T_S) \\ \quad \times \left(-\boldsymbol{u}_i \cdot \nabla d - \dfrac{L_A d}{A_{max}} \right) \Big] \end{array}\right)}{\rho_i \left\{ -L_w + \dfrac{c_i}{2}(T_S - T_B) + c_i d\hat{\kappa}(T_A - T_S) \right\}} \tag{3.8}$$

where

$$\hat{\kappa} = \frac{\kappa_{ia}}{2(\kappa_{ia} d + \kappa_i)}.$$

Details of the derivation of (3.8) are given in Appendix A.

The prognostic equation for A is

$$S_A = H(\xi) \frac{\xi}{\hat{d}} (1 - A) + H(-S_d) \frac{A}{2\hat{d}} S_d, \tag{3.9}$$

where $\xi = S_d$ calculated when $(d = 0)$ and

$$\hat{d} = \begin{cases} d, & d > d_{min} \\ d_{min}, & d \leqslant d_{min}. \end{cases}$$

The first term in eq. (3.9) increases ice concentration by supposing that new ice forming over open water accumulates at a depth d adjacent to existing ice (thereby decreasing the area of ice-free water). The second term is obtained by supposing that the ice thickness is linearly distributed between zero and $2d$. A thermodynamic reduction δd then has an associated reduction $\delta A = A\, \delta d/2d$.

4. Numerical method

4.1. Non-dimensional equations

Following Willmott and Darby (1990), it is readily shown by non-dimensionalizing the momentum equations, that for gyre scale motions on the seasonal (or longer) time scale, the local and inertial acceleration terms can be neglected. It is also convenient computationally to work with a

nondimensional set of governing equations, and so to this end, we define the following dimensionless variables (denoted by primes):

$$L(x', y') = (x, y), \qquad Hh' = h, \qquad Dd' = d,$$

$$U_0(u', v', u_i', v_i') = (u, v, u_i, v_i),$$

$$\frac{DU_0}{L} w' = w, \qquad \frac{L}{U_0} t' = t,$$

$$T_0 T' = T, \qquad S_0 S' = S,$$

$$f_0 f' = f, \tau_0(\tau'_{wa}, \tau'_{ia}, \tau'_{wi}) = (\tau_{wa}, \tau_{ia}, \tau_{wi}),$$

$$\frac{f_0}{L}\beta' = \beta, \qquad (HLf_0U_0)P' = P,$$

$$c_p T_0 L'_w = L_w, \qquad c_p c_i' = c_i,$$

$$f_0 r' = r,$$

$$\frac{\rho_0 c_p U_0 H}{L}(\kappa'_{wa}, \kappa'_{wi}, \kappa'_{ia}) = (\kappa_{wa}, \kappa_{wi}, \kappa_{ia}),$$

$$\frac{1}{D}\hat{\kappa}' = \hat{\kappa},$$

$$\frac{\rho_0 c_p U_0 HD}{L}\kappa_i' = \kappa_i,$$

$$U_0 L(A'_T, A'_S, A'_d, A'_A) = (A_T, A_S, A_d, A_A),$$

$$\frac{U_0 DH}{L} A'_v = A_v, \qquad \frac{U_0}{L}(S'_A, L'_A) = (S_A, L_A),$$

$$\frac{U_0 D}{L} S'_d = S_d,$$

$$\frac{DU_0}{L} w'_e = w_e, \qquad \frac{Lf_0U_0}{T_0Hg}\alpha' = \alpha,$$

$$\frac{Lf_0U_0}{S_0Hg}\gamma' = \gamma, \qquad (\rho_i f_0 U_0 L) S'_m = S_m. \tag{4.1}$$

Substituting (4.1) into (2.1)–(2.6), (3.1)–(3.4), (3.8) and (3.9) and dropping the primes gives:

$$\varepsilon\left\{\frac{\partial(hu)}{\partial t} + \nabla\cdot(hu\boldsymbol{u})\right\} - fvh = -\frac{\partial P}{\partial x} - \frac{2\delta P}{h} A\frac{\partial d}{\partial x} + \eta_1[(1-A)\tau^x_{wa} + A\tau^x_{wi}] - ruh, \tag{4.2}$$

$$\varepsilon\left\{\frac{\partial(hv)}{\partial t} + \nabla\cdot(hv\boldsymbol{u})\right\} + fuh = -\frac{\partial P}{\partial y} - \frac{2\delta P}{h} A\frac{\partial d}{\partial y} + \eta_1[(1-A)\tau^y_{wa} + A\tau^y_{wi}] - rvh, \tag{4.3}$$

$$\frac{\partial h}{\partial t} + \nabla\cdot(\boldsymbol{u}h) + \delta(w - w_e) = 0, \tag{4.4}$$

$$\frac{\partial(hT)}{\partial t} + \nabla\cdot(\boldsymbol{u}hT) = -(1-A)Q_{wa} - AQ_{wi} - Q_{FR} + \delta(w_e - wT_B) + A_T\nabla\cdot(h\nabla T) + \delta\frac{\rho_i}{\rho_0} dS_A \times\left\{L_w + c_i\left(\frac{T_B - T_S}{2}\right)\right\}, \tag{4.5}$$

$$\frac{\partial(hS)}{\partial t} + \nabla\cdot(\boldsymbol{u}hS) = \delta(w_e - wS_i) + A_S\nabla\cdot(h\nabla S), \tag{4.6}$$

$$\varepsilon\left\{\frac{\partial(\mathrm{d}u_i)}{\partial t} + \nabla\cdot(du_i\boldsymbol{u}_i)\right\} - fv_i d = \eta_2(\tau^x_{ia} - \tau^x_{wi}) - S_m\frac{\partial(\mathrm{d}A)}{\partial x}, \tag{4.7}$$

$$\varepsilon\left\{\frac{\partial(\mathrm{d}v_i)}{\partial t} + \nabla\cdot(dv_i\boldsymbol{u}_i)\right\} + fu_i d = \eta_2(\tau^y_{ia} - \tau^y_{wi}) - S_m\frac{\partial(\mathrm{d}A)}{\partial y}, \tag{4.8}$$

$$\frac{\partial(Ad)}{\partial t} + \nabla\cdot(Ad\boldsymbol{u}_i) = AS_d + dS_A + A_d\nabla\cdot(A\nabla d), \tag{4.9}$$

$$\frac{\partial A}{\partial t} + \nabla\cdot(A\boldsymbol{u}_i) = S_A + L_A + A_A\nabla^2 A, \tag{4.10}$$

$$S_d = \frac{NUM}{DEN}, \tag{4.11}$$

$$S_A = H(\xi)\frac{\xi}{\hat{d}}(1-A) + H(-S_d)\frac{A}{2\hat{d}}S_d, \tag{4.12}$$

where

$$NUM = \frac{\rho_0}{\delta\rho_i}\left\{\frac{Q_{FR}}{A} + Q_{wi} - Q_{ia}\right\}, - c_i d\left[d\hat{\kappa}\frac{\partial T_A}{\partial t} + \boldsymbol{u}_i\cdot\nabla\left(\frac{T_S + T_B}{2}\right) + \hat{\kappa}(T_A - T_S)\left(-\boldsymbol{u}_i\cdot\nabla d - \frac{L_A d}{A_{max}}\right)\right],$$

$$DEN = -L_w + \frac{c_i}{2}(T_S - T_B) + c_i\, d\hat{\kappa}(T_A - T_S),$$

$$P = \frac{1}{2}h^2[\alpha(T-1) - \gamma(S-1)],$$

$$Q_{FR} = H(T_B - T)\left[\frac{h(T-T_B)}{2\Delta t} - (1-A)Q_{wa}\right],$$

$\eta_1 = \tau_0/(\rho_0 f_0 U_0 H)$, $\eta_2 = \tau_0/(\rho_i f_0 U_0 D)$, $f = 1 + \beta y$, $\delta = D/H$ and $\varepsilon = U_0/f_0 L$ is the Rossby number. Typical values are $U_0 = 0.05\ \mathrm{ms}^{-1}$, $f_0 = 10^{-4}\ \mathrm{s}^{-1}$, $L = 10^6$ m, $H = 100$ m and $D = 1$ m, which give $\varepsilon = 5 \times 10^{-4}$ and $\delta = 10^{-2}$. Therefore, in (4.2), (4.3), (4.7) and (4.8), we neglect the terms of $O(\varepsilon)$ but we always retain $O(\delta)$ terms since they may become significant for interannual time scale solutions.

4.2. *Numerical scheme*

Equations (4.2)–(4.12) are solved numerically in a meridionally aligned channel. Since $\Delta x > r_i$, where r_i is the internal Rossby radius and Δx is the grid size, we employ a finite difference B-grid (see Batteen and Han, 1981). The B-grid combined with the flux form of equations (4.4), (4.5), (4.6), (4.9) and (4.10) ensures global conservation (except at open boundaries) of active layer mass, heat and salt and ice mass and concentration respectively. The details of our finite-difference scheme closely follow Haney (1974). We use a central difference time-step with a 5% linear average back in time every time-step to prevent leap-frog instability. The horizontal diffusion terms are simply lagged in time for numerical stability. The terms involving S_m in (4.7) and (4.8) are also lagged in time because when this pair of equations are used to eliminate u_i and v_i in (4.9), diffusive terms in d arise which contain the factor S_m. The results presented in this paper were computed on a 45×45 regular grid. The (nondimensional) domain is defined by $0 \leqslant x \leqslant 1$ and $-1 \leqslant y \leqslant 1$. Experiments with various grid spacings indicate that $\delta t = 0.5(\delta x)^2$ is necessary for satisfactory numerical solution. This is consistent with the diffusive term involving S_m (discussed above) controlling the maximum size of the time step.

When ice is present the four eqs. (4.2), (4.3), (4.7) and (4.8) are solved simultaneously for (u, v) and (u_i, v_i) using Newton iteration. After the first time step we usually find that one iteration is sufficient.

Preliminary experiments with realistic forcing fields and boundary conditions led to solutions which included regions of negative P and therefore correspond to convectively unstable regions. Although a reduced gravity model cannot correctly model vertical mixing, we believe it is valuable to include a simple parameterization of this important process (see Killworth 1979, 1983 and Häkkinen et al., 1992). Thus wherever $P \leqslant 0$ occurs, we completely mix the column, which in practise means that the active layer temperature and salinity instantly adopt the values of the abyssal region. Since there is now no vertical stratification at such points the concept of active layer depth has no meaning. We assume that the strong convective adjustment eliminates the mixed layer which then quickly reforms to some shallow value on the Pollard-Rhines-Thompson short time-scale (Pollard et al., 1973) of one half of the inertial period. Specifically this is parameterized by simply setting $h = 20$ m after mixing has occurred. We also note that setting h to a shallow value at a point where $P = 0$ is consistent with the fact that convection occurs near the centre of the cyclonic gyre in this model.

The model results demonstrate that this convective scheme has a realistic effect on the ice cover, but it is worthwhile to consider the processes which set the final size of an open ocean convection region. Killworth (1979) suggests convection may occur in narrow "chimneys" of intense mixing, the horizontal length scale being set by preconditioning on the internal Rossby radius length scale. In the model presented here, a convectively unstable region will tend to increase in size due to diffusion of salt out of the region and cooling, whereas the size will be limited (or reduced) due to diffusion of heat out of the region, warming and the advection of low density water into the region. We have usually found that, once initiated, a convectively unstable region grows, primarily via salinity diffusion, until the boundary of the region first encounters a non-closed streamline. At this stage, advection can remove the salt diffusing out of the region. Therefore, if upwelling at the centre of a cyclonic gyre has played a role in preconditioning a region to become unstably stratified (as it does in our results) the convectively unstable region which

develops grows relatively large compared with internal deformation scale "chimneys". However, on the gyre length scale and seasonal (or longer) time scales for which our model is formulated we believe that the convective scheme used here provides a useful parameterization of the open ocean convection (see, Crépon et al. (1989) and Gascard (1990) for a discussion of this problem).

It is interesting to speculate whether the processes which limited the eventual size of the Weddell Sea polynya (an interannual time scale feature with a horizontal length scale which is an order of magnitude larger then the internal deformation radius) were similar to those which limit the size of convectively unstable regions in this model. Ou (1991) and Häkkinen et al. (1992) suggest that the length scale of regions which are preconditioned for overturning may be determined by topographic features.

4.3. *Boundary conditions*

The channel is bounded by insulating rigid walls at $x = 0, 1$ along which the no-normal flow condition is applied to both the ocean and ice velocity fields. We also require boundary conditions for h, T, S, Ad and A on the open zonal boundaries $y = \pm 1$. Consider first the boundary condition for h. The transport components hu and hv in (4.4) are eliminated using (4.2) and (4.3) to give a single equation for h. On the open zonal boundaries an approximate form of this equation is

$$\frac{\partial h}{\partial t} = \frac{\beta}{f^2}\frac{\partial P}{\partial x} + \frac{r}{f^2}\frac{\partial^2 P}{\partial x^2} - \delta w + \delta w_e - \eta_1 \boldsymbol{k} \cdot \mathrm{curl}\left[\frac{(1-A)\boldsymbol{\tau}_{wa} + A\boldsymbol{\tau}_{wi}}{f}\right], \qquad (4.13)$$

where we have retained only the largest term involving r. Note that (4.13) contains no y derivatives (with the exception of known shear stress terms) permitting easy solution for h on $y = \pm 1$. Care is required in the choice of h at the four corners. The steady-state analytical solution of the purely dynamical wind-driven ocean circulation model only requires a value of P somewhere on the eastern boundary and a specification of the net meridional transport. By analogy, in the numerical model we find it appropriate to choose $P(1, -1, t) = P_0$, where P_0 is some constant. We choose $P_0 = P(1, -1, 0)$. Knowledge of $T(1, -1, t)$ and $S(1, -1, t)$ then gives $h(1, -1, t)$. The values of $h(0, -1, t)$ and $h(1, 1, t)$ are chosen to imply $u = 0$ on the rigid walls. Finally we choose $h(0, 1, t)$ to impose a specified net meridional transport, M, across the line $y = 1$.

The open boundary conditions described by Stevens (1990) are applied to T and S on $y = \pm 1$. Briefly, this involves specifying T and S on the boundary where v is into the domain. Otherwise a meridional phase speed c_s (associated with either T or S just inside the domain) is calculated and interior information is propagated onto the open boundaries at a speed $v + c_s$. If v_i is out of the domain then Ad and A are treated in the same manner as T and S. Otherwise the fluxes of $v_i Ad$ and $v_i A$ are specified on the open boundary (this is not equivalent to specifying A and d on the open boundary). In this model, ice always exits the domain across the open boundary $y = -1$.

5. Results

5.1. *Forcing fields*

In this section we demonstrate the model behaviour by describing two experiments. The parameters are designed to simulate the Greenland-Norwegian sea. The fields $T_A(x, y)$, $T(x, -1)$, and $\boldsymbol{\tau}(x, y) = (\tau^x, \tau^y)$ are based on those used by WM. Unless otherwise stated we choose:

$$T_A(x, y) = 7.5 - \frac{67.5}{\pi}\tan^{-1}\left(\frac{1+y}{x + 2/\sqrt{3}}\right) \ (^\circ\mathrm{C}),$$

$$\tau^x = -\tau_0 \cos(\theta)\cos\left[\frac{\pi}{R_L}\left(\frac{y - x\tan\theta + l}{1+l}\right)\right] \times \mathrm{Nm}^{-2},$$

$$\tau^y = -\tau_0 \sin(\theta)\cos\left[\frac{\pi}{R_L}\left(\frac{y - x\tan\theta + l}{1+l}\right)\right] \times \mathrm{Nm}^{-2}, \qquad (5.1)$$

$$T(x, -1, t) = \begin{cases} (34 - 10x)/3, & 0.7 \leqslant x \leqslant 1 \\ 7.25 + 2.5x, & 0.3 \leqslant x \leqslant 0.7 \\ 6 + 20x/3, & 0 \leqslant x \leqslant 0.3, \end{cases} \ (^\circ\mathrm{C}) \qquad (5.2a)$$

$$T(x, 1, t) = -1.5 + x \ (^\circ\mathrm{C}), \qquad (5.2b)$$

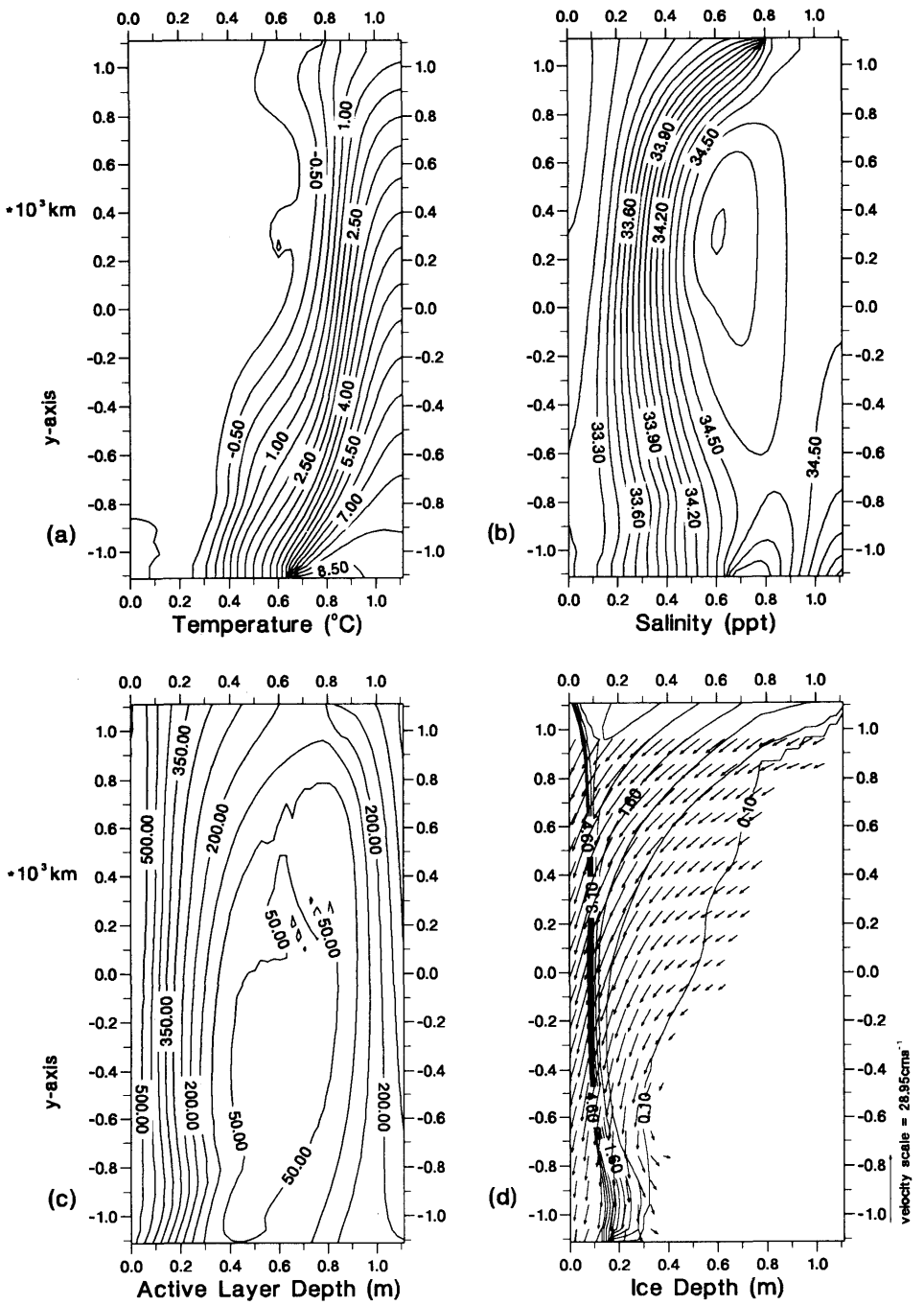

Fig. 1. Contours of (a) T; (b) S; (c) h; (d) ice depth d; (e) A; (f) P in the steady state at $t = 30$ years. Ice velocity and ocean velocity vectors are superimposed on (d) and (f) respectively. On the open boundaries the salinity distributions approximate the annually averaged salinity given by Levitus (1986) at these latitudes. The air-ice drag coefficient, c_{ia}, and air-ocean drag coefficient, c_D, in the shear stress parameterisations are identical in size.

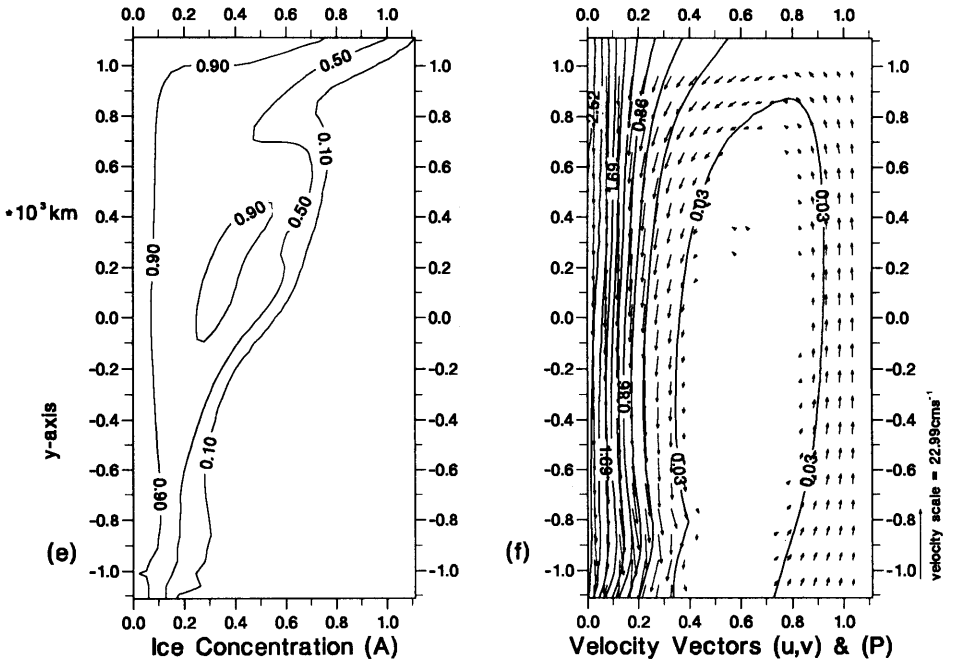

Fig. 1. (Continued).

$$S(x, -1, t) = \begin{cases} S_S, & 0 \leqslant x \leqslant x_S \\ S_S - \dfrac{(x - x_S)}{(1 - x_S)}(S_S - 34), & \\ & x_S \leqslant x \leqslant 1, \text{ (ppt)} \end{cases} \tag{5.3a}$$

$$S(x, 1, t) = S_N - x(S_N - 34), \quad 0 \leqslant x \leqslant 1 \text{ (ppt)} \tag{5.3b}$$

$$v_i A = -0.15 A_{max}(1 - 0.9x), \text{ (ms}^{-1}\text{)} \quad \text{at} \quad y = 1, \tag{5.4}$$

and in order to specify the flux $v_i Ad$ at $y = 1$, we specify $d(x, 1, t)$ to be a piecewise linear distribution between $d(0, 1, t) = 2.0$, $d(0.33, 1, t) = 2.0$ and $d(1, 1, t) = 1.2$, where the units are in metres. All the remaining parameter values are listed in Appendix B. Note that in (5.1)–(5.3), with the exception of x and y, we have reverted to dimensional units. If we set $S_S = 34.9$ ppt, $x_S = 0.7$ and $S_N = 33$ ppt, then expressions (5.3) are approximate parameterizations of the annually averaged salinity given by Levitus (1986). The values of f_0 and β correspond to a β-plane centred at 70°N. The parameter $A_{max} = 0.98$ ensures a minimum of 2% open water parameterizing the increased heat loss through leads. The ocean model is initialized with a uniform motionless state with $h = 200$ m, $T = 7$ °C and $S = 34$ ppt. The ice model is initialized with uniform ice cover $A = A_{max}$ and $d = 2$ m.

We present results from two experiments which clearly demonstrate the model response to seasonally varying air temperatures, variations in S_N (the northern salinity boundary conditions) and c_{ia} (the ice-air drag coefficient that appears in the ice-air shear stress formulation).

We define, $\tilde{T}_A(x, y, t)$, a seasonally varying atmospheric temperature field as

$$\tilde{T}_A(x, y, t) = T_A(x, y) - \hat{T}_A \cos(2\pi t_y), \tag{5.5}$$

where t_y represents time in years and $\hat{T}_A$ is a constant.

Experiment no. 1

Throughout this experiment we set $c_{ia} = 1.2 \times 10^{-3}$ so that $c_{ia} = c_D$. The complete run from 0 to 60 years divides into 4 sections:

(i) 0 to 30 years consists of a spin-up during which $S_S = 34.9$ ppt, $x_S = 0.7$, $S_N = 33$ ppt and $\hat{T}_A = 0$.

(ii) At 30 years, we set $\hat{T}_A = 7\,^\circ$C and integrate the model for a further 15 years. During this phase, the time-dependent air temperature forcing leads to a small convection region which appears in spring and disappears in the autumn. According to Mysak et al. (1990) normal winter/spring conditions in the Greenland Sea have a number (as yet unknown) regions of convection. As the GSA is advected through the domain Mysak et al. (1990) speculate that convection is "switched off". The 45th year of the model integration thus captures "typical" Greenland Sea conditions.

(iii) At 45 years, S_N is changed from 33.0 to 32.0 ppt and the model is integrated for a further 5 years. This stage of the integration simulates a period of anomalously fresh northern inflow water (the GSA).

(iv) At 50 years, S_N is returned to 33.0 ppt and the model is integrated to 60 years.

Fig. 1 shows steady-state solutions of the T, S, h, d (and $\boldsymbol{u}_i$), A and P (and $\boldsymbol{u}$) fields respectively. The ocean flow consists of a cyclonic gyre with an equatorward flowing western boundary current (the EGC). At the extreme southern tip of Greenland the EGC has a transport of approximately 14 Sv (see Worthington, 1970; McCartney and Talley, 1984) which is close to the value $M = -13$ Sv chosen to give a realistic flow in this model (recall that M is the total net meridional transport and not the meridional transport of the boundary current the latter of which depends on latitude). The active layer is shallow at the centre of the cyclonic gyre where the terms containing w_e are important, leading to entrainment of abyssal water into the active layer. Thus, there is a salinity maximum at the centre of the cyclonic gyre produced by entrainment of salty abyssal water.

The cold northerly air temperature causes the warm southerly inflow to rapidly cool as it is advected northwards by the flow. Eventually ice occurs, either through thermodynamic local ice production or via advection of equatorwards moving ice which enters at the northern boundary. The ice cover insulates the water column from the cold air above and hence beneath the ice the ocean temperature field is almost isothermal (a general feature of all solutions). Columns of fluid, once subducted beneath the ice, are insulated from the cold air temperatures and horizontal diffusion of heat then acts to produce an approximately isothermal ocean temperature field. On the southern boundary, a temperature front separates warm inflow from the cold outflow of the East Greenland Current (EGC). Similarly, a temperature front exists on the northern boundary separating the relatively warm outflow from the cold inflow. The position and magnitude of the temperature front on the northern boundary is in good agreement with observations across Fram Strait at 79°N shown by Manley et al. (1987). Notice that large regions exist where $T < T_0$ but since $S < S_0$, it is possible for the active layer to remain stably stratified. However, as high salinity water columns travel northwards they cool and may become convectively unstable. This leads to a small region of convection at the centre of the salinity maximum, which accounts for the deviation of the $T = -1\,^\circ$C contour and the noisy $h = 50$ m contours in this region.

The ice depths generally have a northeast-southwest orientation, increasing to about 2.0 m in the northwest corner. The ice flow is generally in a southwesterly direction which results (via convergence once $A = A_{max}$) in large ice depths close to the western boundary layer. The southward flow of ice close to the western boundary allows the ice cover to extend to the southwest corner. If we interpret the western boundary of our idealized domain as the east coast of Greenland then the general features of the solution mentioned above are realistic, except that the ice depths are too large close to the western boundary. These unrealistic, large ice depths are due to the parameter S_m (see (3.1), (3.2)) being set to a small value (compared with Semtner, 1987) and the idealized western boundary geometry. Experiments (not shown) with larger values of S_m resulted in a wider western boundary layer in the ice velocity field and correspondingly reduced ice depths near the western boundary. However, the disadvantage of using larger values of S_m is that in the southwest corner the ice extends further eastward which leads to a significant mass of ice becoming recirculated by the cyclonic ocean flow. In reality, south of approximately 70°N the east coast of Greenland has a southwest-northeast orientation. It is possible that a future model which adopts the realistic east Greenland coastline will prevent the convergence and subsequent ice build-up, against

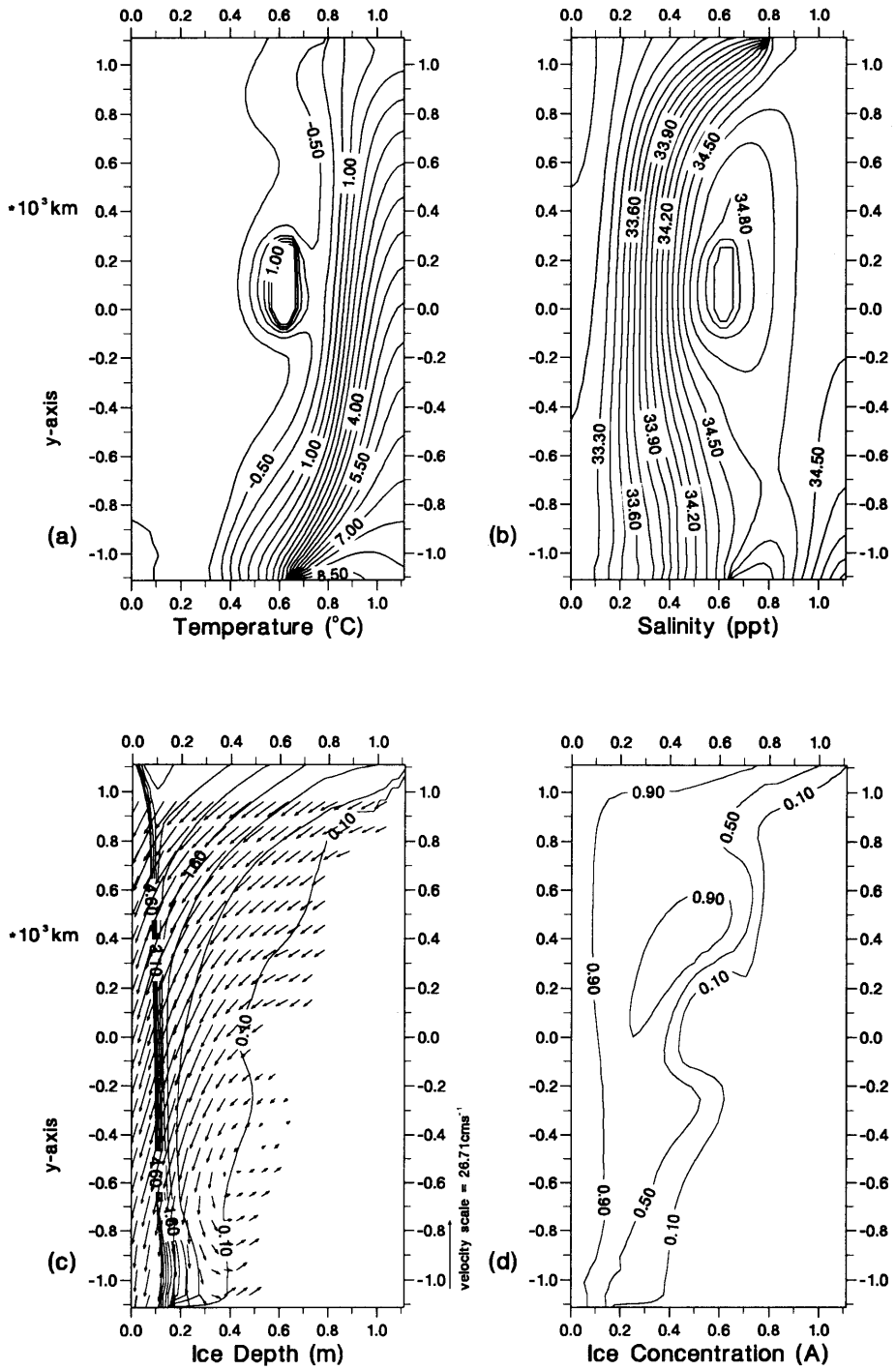

Fig. 2. Contours of (a) T; (b) S; (c) d; (d) A for a typical Spring. Ice velocity vectors are superimposed on (c).

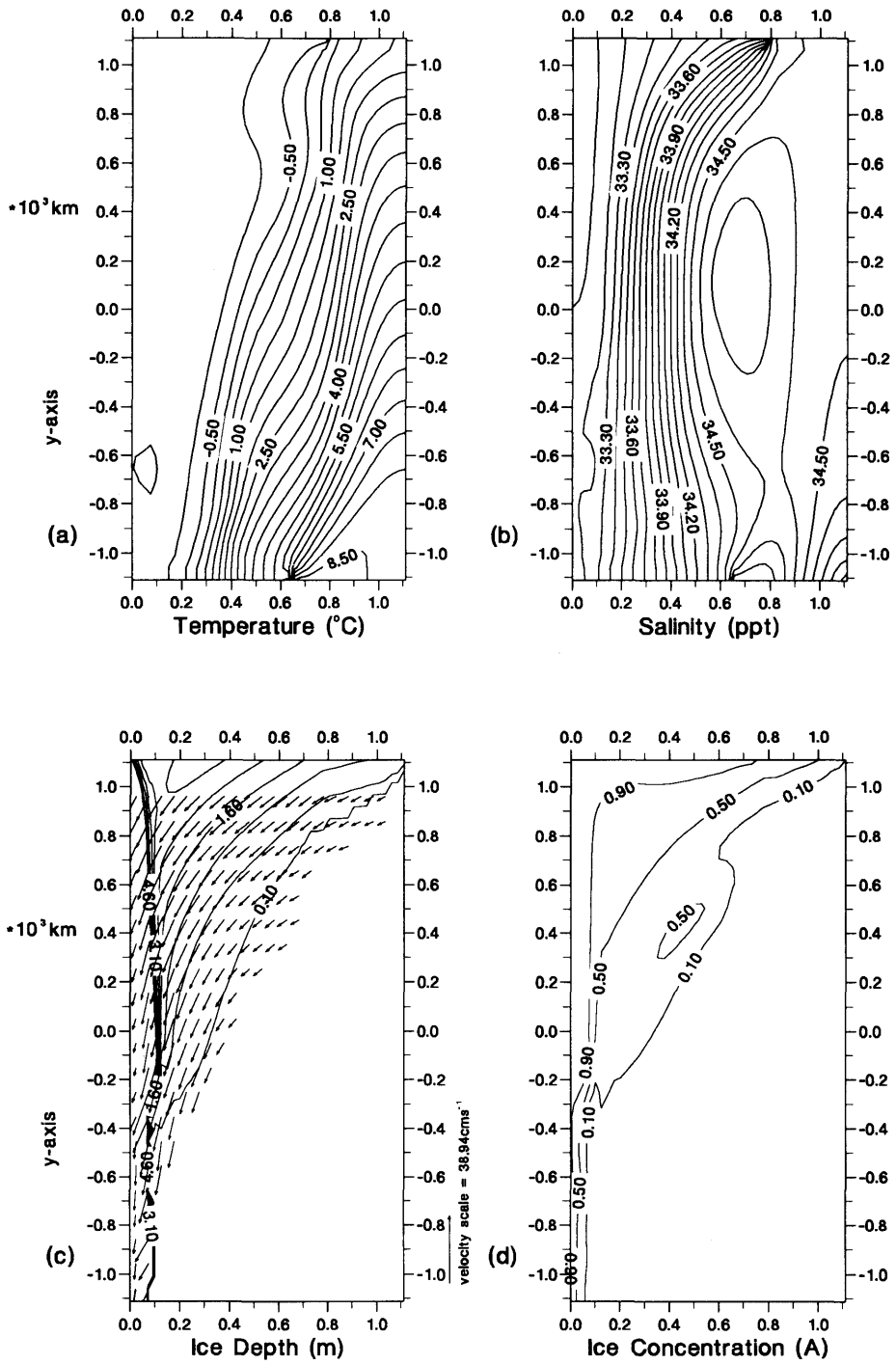

Fig. 3. As in Fig. 2 except for a typical Autumn.

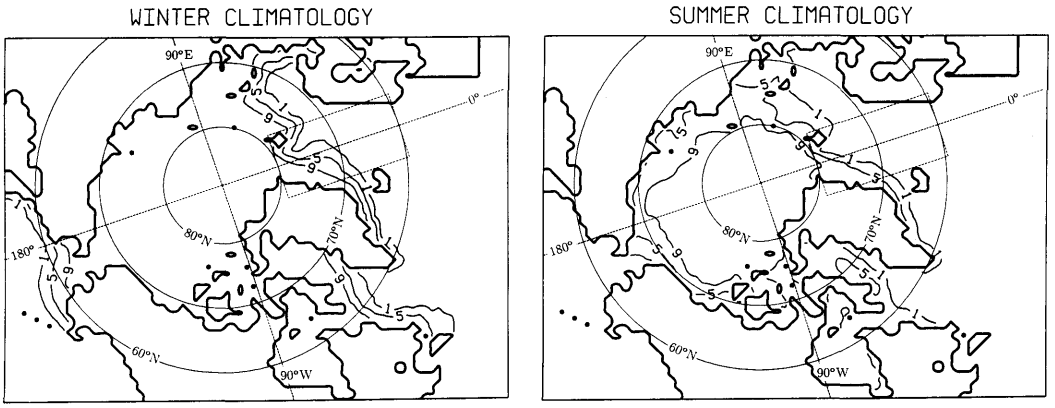

Fig. 4. Winter and Summer ice concentration climatologies calculated during the period 1953–1984 (from Manak and Mysak, 1987). The labels 1, 5 and 9 denote 10%, 50% and 90% ice concentration respectively. The dashed box represents the model domain in the Greenland-Norwegian Sea and extends from 60°N to 80°N and 15°W to 15°E.

the western boundary. Indeed since the interior ice velocities are orientated almost parallel to the east Greenland coastline south of 70°N we would expect to see relatively small amounts of ice convergence in this region.

The ice concentration contours exhibit interesting structure; the 0.1 contour closely follows the 0.1 m ice depth contour whereas the 0.5 and 0.9 ice concentration contours clearly reveal the intrusion of the warm water advected by the cyclonic gyre. The general position and shape of the 0.1 and 0.5 ice concentration contours compares well with annual climatology for ice concentration given by Manak and Mysak (1987). The isolated region of ice concentration in excess of 0.9 which occurs close to the ice edge is discussed below.

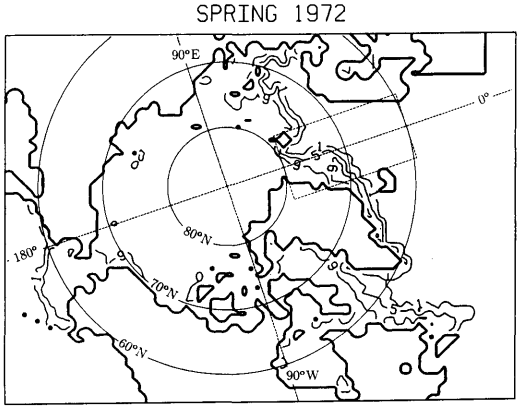

Fig. 5. Observed Spring 1972 ice concentration field, from Manak and Mysak, 1987.

We now describe the solutions for sections (ii)–(iv) of this experiment, which are forced by a seasonally varying atmospheric temperature field, together with an altered northern boundary salinity. The latter forcing is chosen to simulate the "GSA event" that occurred during the 1960s and which is discussed by Mysak et al. (1990) and Marsden et al. (1991). These two papers demonstrate a correlation between anomalous regions of low salinity water and large amounts of winter ice in the Greenland and Labrador Seas. It is proposed that during periods characterized by cool relatively fresh water, convection is inhibited, thus preventing the mixing of warm deep water with cold surface water and leading to a larger ice extent.

Fig. 2 shows the T, S, d (and $\boldsymbol{u}_i$) and A fields at 44.25 years, and represents typical spring conditions once an annual signal has been established by the time dependent air temperature forcing. The analogous results at 44.75 years (autumn of the final year) are shown in Fig. 3. Contours of A obtained from the model contain features similar to the observed variations of A discussed by Manak and Mysak (1987) some of which are reproduced in Figs. 4, 5. Fig. 4 shows observations of climatological A in winter (average of December, January and February) and summer (average of June, July and August) calculated by Manak

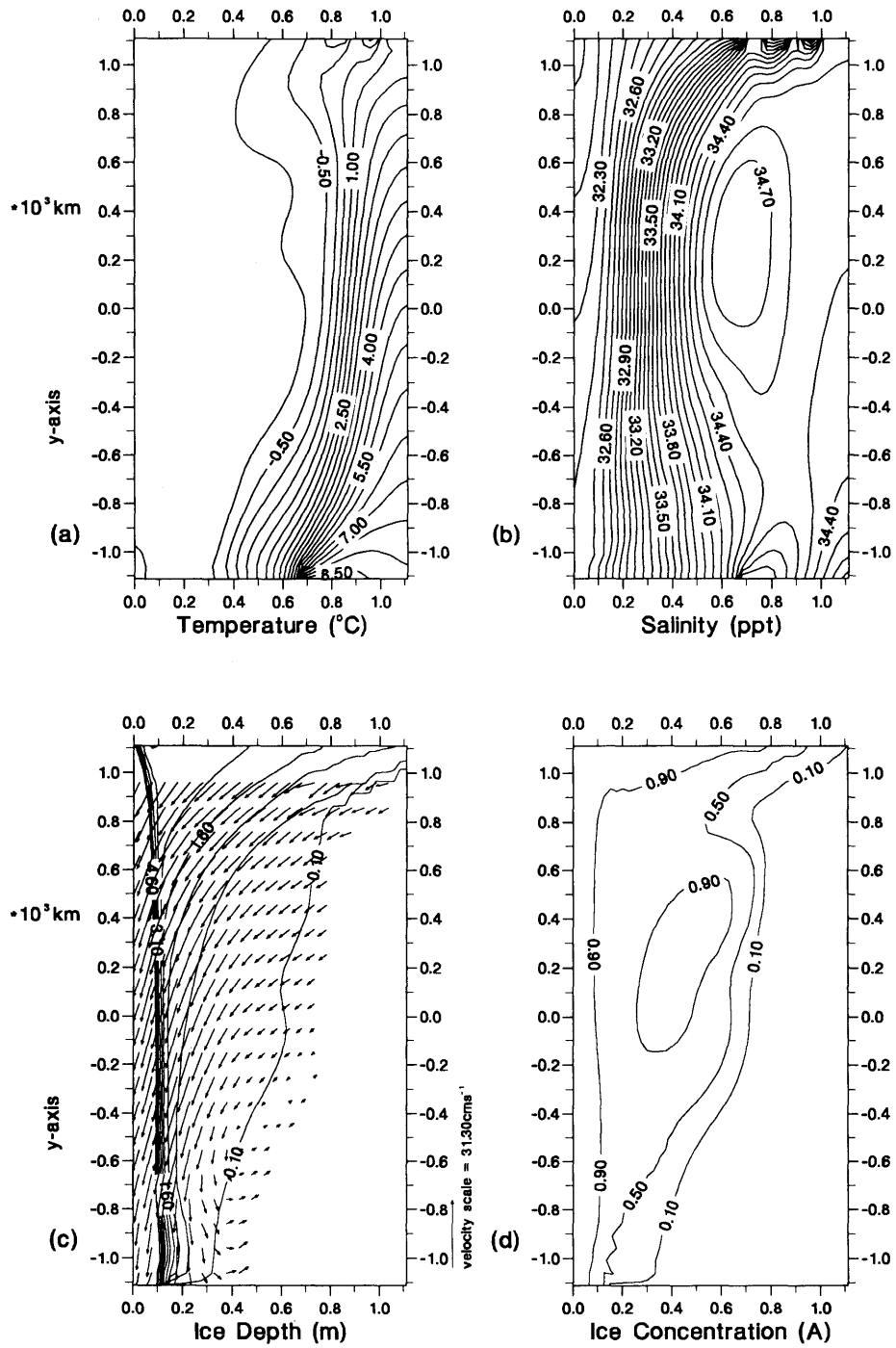

Fig. 6. As in Fig. 2 except that the solutions correspond to anomalous Spring conditions when the northern boundary salinity is freshened, thereby supressing convection.

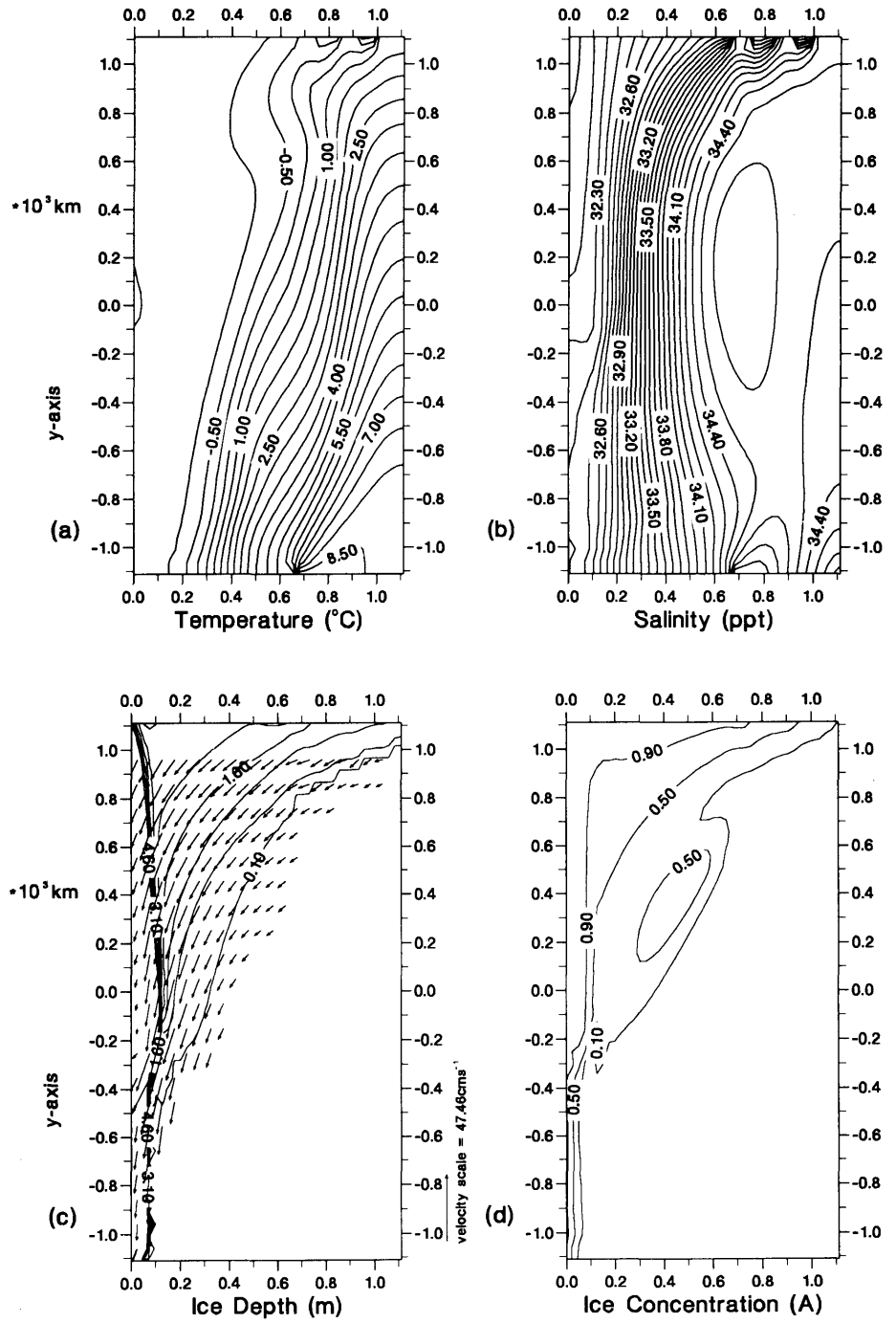

Fig. 7. As in Fig. 3 except that the solutions correspond to anomalous Autumn conditions when the northern boundary salinity is freshened. Since there is no convection region in Fig. 3, the difference between these two sets of solutions is small.

and Mysak (1987). Observations of A in spring (average of March, April and May) for 1972 calculated by Manak and Mysak (1987) are reproduced in Fig. 5. Fig. 2d shows that in spring the A contours are closely spaced near the ice edge whereas in autumn (see Fig. 3d) the ice concentration contours are more widely spaced with less structure. In particular, the isolated region of $A > 0.9$ has disappeared. It is interesting to note that although winter and spring climatology, from the Manak and Mysak (1987) atlas, do not show isolated regions of $A > 0.9$, spring in individual years does sometimes contain this feature. For example, the A contours for spring 1972 shown in Fig. 5 illustrate this point well, where an isolated region with $A > 0.9$ exists, in good agreement with our model solutions.

Notice that variations in atmospheric temperature lead to an enlarged convectively unstable region in spring (in response to enhanced ocean cooling to the atmosphere), whereas there is no convection in autumn. As ice attempts to advance equatorward in the autumn, sea water freezes around the perimeter of the convecting region (see Fig. 2d) thereby producing a tongue-like feature centred at approximately 71° N. Wadhams (1992) reports that at this latitude a tongue of ice (known as the Odden tongue) forms during the winter and persists until early April in most years.

Ice depths only vary significantly close to the ice-edge. The P, h (not shown) and S fields show insignificant response to the atmospheric temperature forcing.

We now discuss solutions for section (iii) of this experiment. Figs. 6, 7 show the show the T, S, d and A fields at 49.25 and 49.75 years corresponding to spring and autumn respectively in the final year of integration with anomalous low northern boundary salinity. The low salinity inflow on the northern boundary results in the suppression of the winter convection region which in turn affects the ocean temperatures and hence the ice edge. This is most clearly seen by comparing the A contours in 2d with 6d.

Mysak et al. (1990) show a time-series (Fig. 6) of temperature and salinity anomalies in June at 25 m depth at 67–69° N, 11–15° W for 1950–1974. The GSA is regarded as beginning in 1968 when salinity was about 34.2 ppt and temperature about 0 °C, as opposed to previous mean values of 34.8 ppt and 2.32 °C respectively. The heaviest ice conditions in the Greenland sea since 1902 (see Mysak et al. (1990)) also occurred in the 1967–1968 period. These observations are qualitatively reproduced in our simulation. In the convectively unstable region of Fig. 2 (centred at approximately 70° N, 1° E) the temperature is 2 °C and salinity is 35 ppt as opposed to the same region in Fig. 6 (a period of anomalous large ice cover) when temperature is approximately −0.5 °C and salinity is approximately 33.8 ppt. Thus, quantitatively this simple model also does remarkably well at simulating the interannual ice distribution described by Mysak et al. (1990). As expected, there is not such a dramatic difference between the autumn solutions in the "normal" and "GSA-period" (see Figs. 3, 7, respectively).

Experiment no. 2

This experiment is identical to experiment no. 1 except $c_{ia} = 2.0 \times 10^{-3}$ which leads to enhanced shear stress at the air-ice and ice-ocean interfaces. For brevity, the steady state solutions at 30 years are not shown. Instead we contrast the behaviour of the model during the spin-up regime in experiment nos. 1 and 2 by examining a time-series of the total ice volume from 5 years to 30 years, shown in Fig. 8. It is interesting to note that when the magnitude of the ice-air shear stress is increased the ice volume undergoes interannual oscillations as the model adjusts towards a steady-state. We believe that this may be due to the following feed-

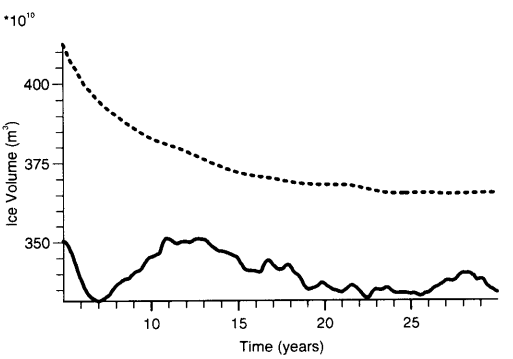

Fig. 8. Time series of total ice volume from 5 to 30 years for the spin-up of experiment no. 1 where $c_{ia} = c_D = 1.2 \times 10^{-3}$ (broken line) and the spin-up experiment no. 2 where $c_{ia} = 2.0 \times 10^{-3}$ and $c_D = 1.2 \times 10^{-3}$ (solid line). We refer to experiment no. 2 as the ice enhanced stress case.

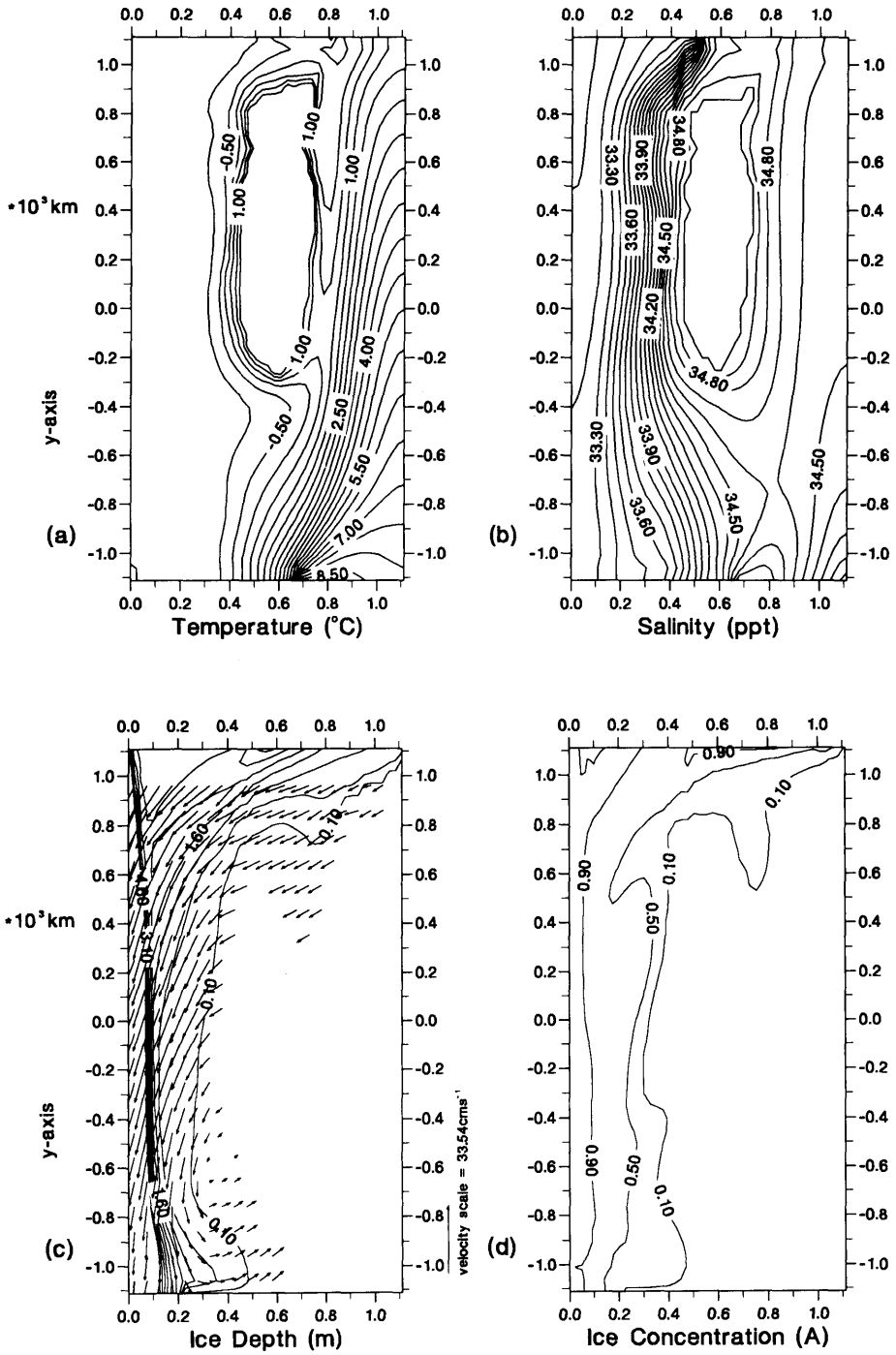

Fig. 9. Contours of (a) T; (b) S; (c) d; (d) A for a typical Spring in the ice enhanced stress case. Ice velocity vectors are superimposed on (c).

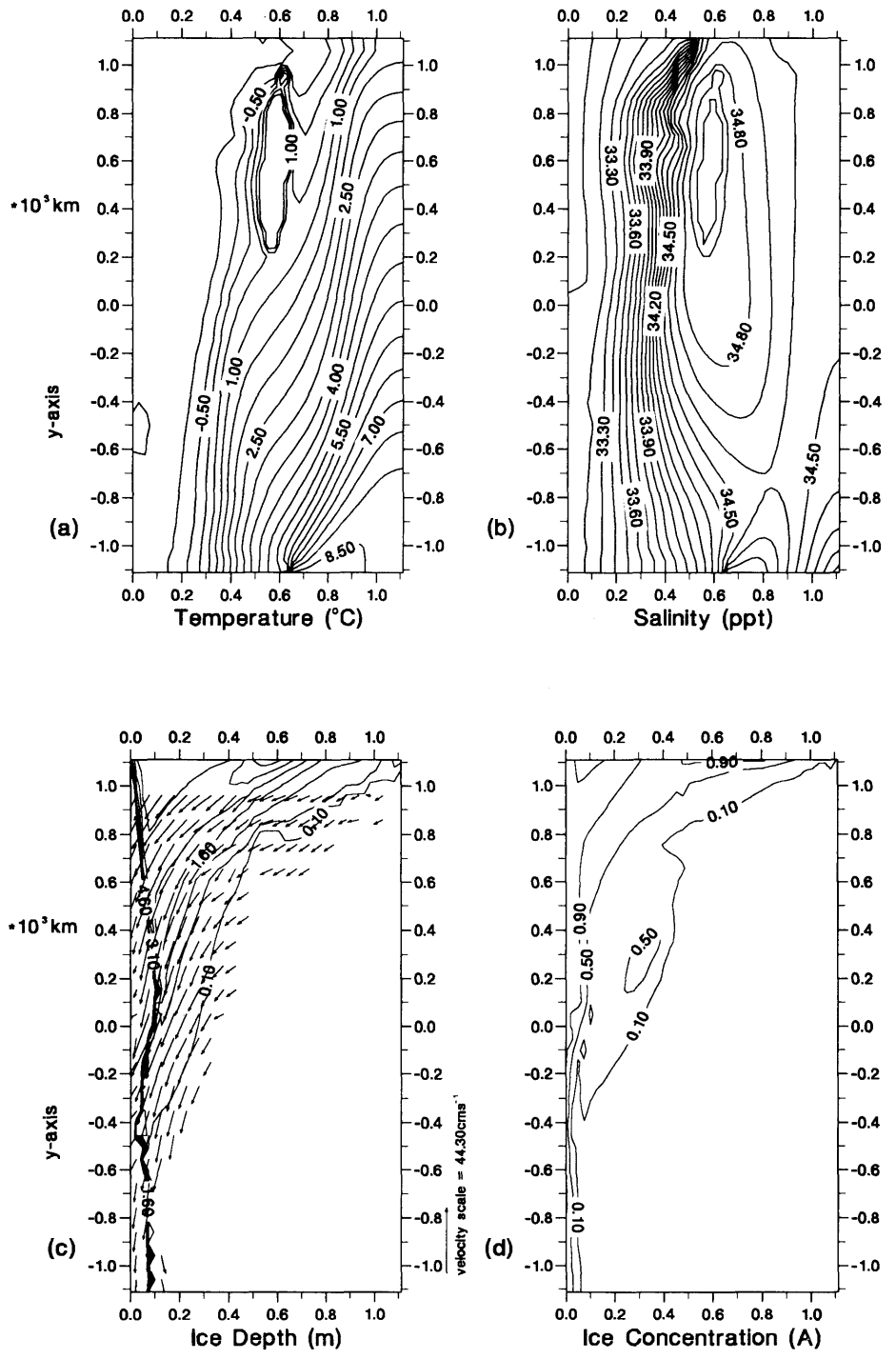

Fig. 10. As in Fig. 9 except for a typical Autumn.

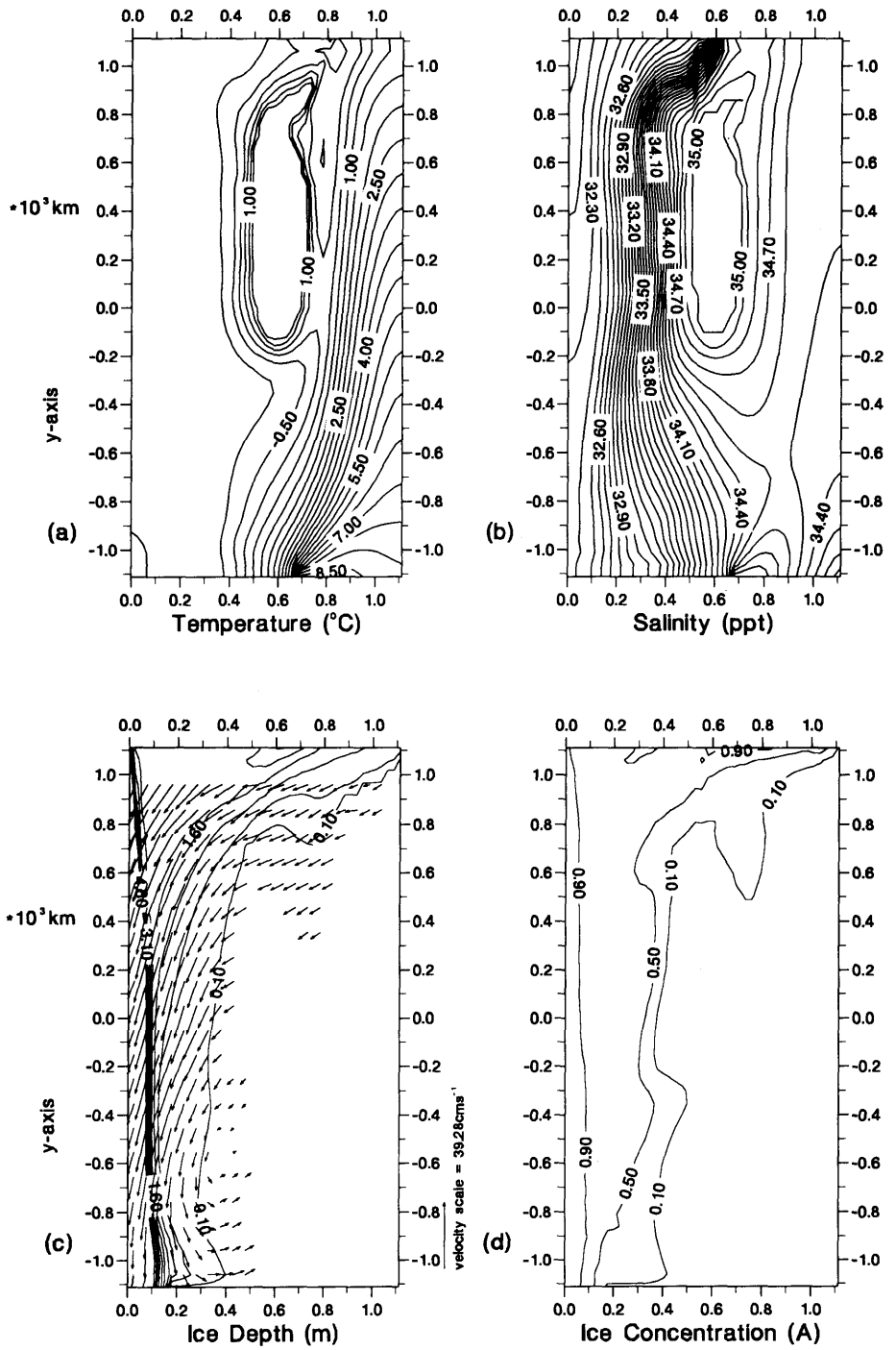

Fig. 11. As in Fig. 9 except for anomalous Spring conditions when the northern boundary salinity is freshened. The size of the convection region has been reduced compared with that in Fig. 9.

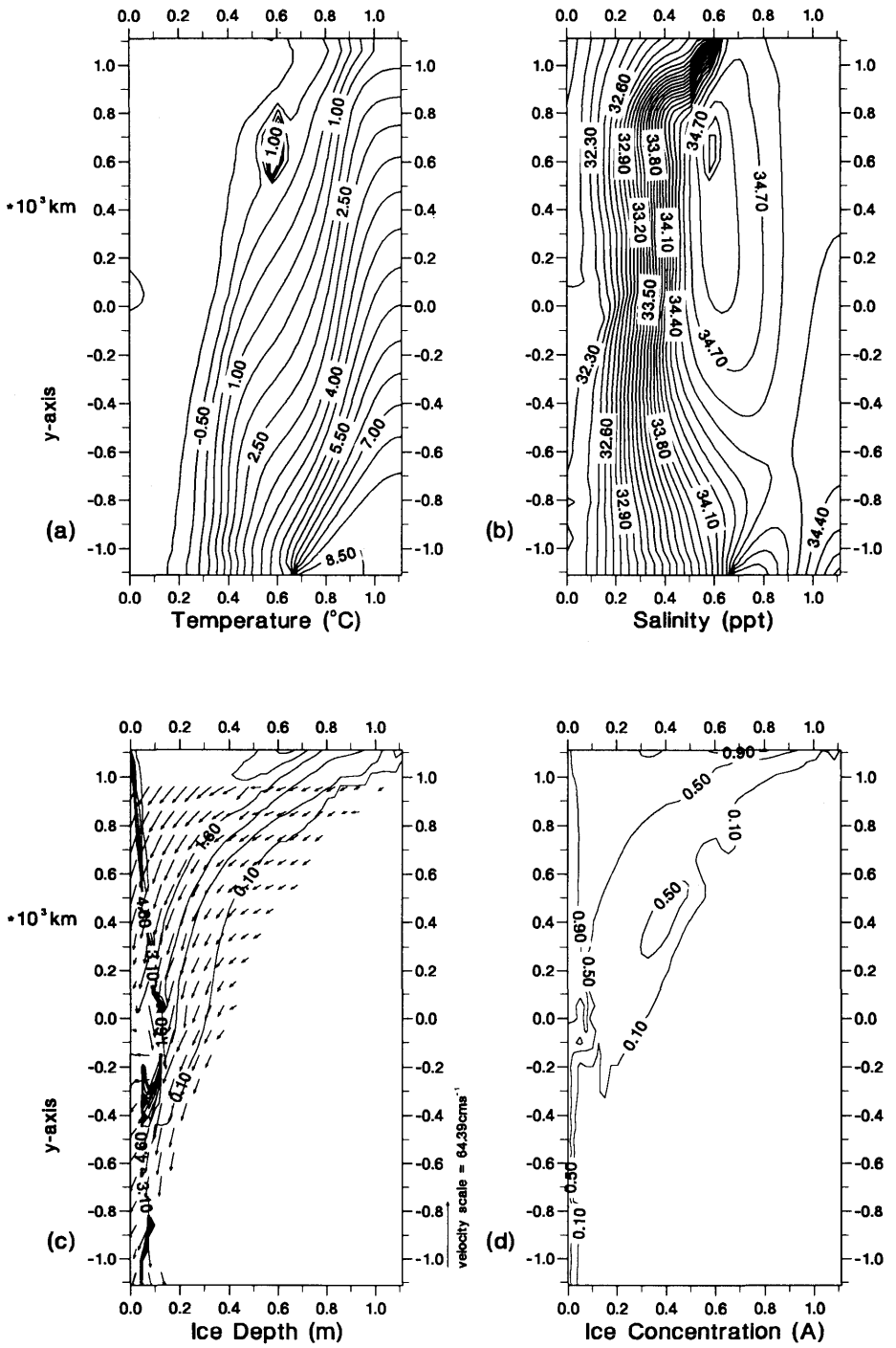

Fig. 12. As in Fig. 10 except for anomalous Autumn conditions when the northern boundary salinity is freshened. A small convection region is still present and should be compared with that in Fig. 10.

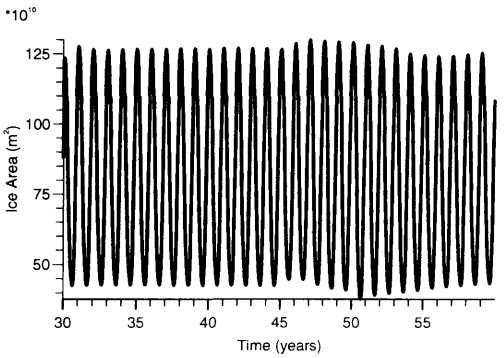

Fig. 13. Time series of total ice area from 30 years to 60 years for experiment no. 1.

back process; as ice forms the ice-air shear stress is increased and hence the water-ice shear stress will tend to increase. This in turn will result in a polewards extension of the region preconditioned for convection which will bring warm water to the surface, melt the newly formed ice and reverse the process.

Figs. 9, 10 show solutions at 44.25 and 44.75 years corresponding to spring and autumn in the final year, respectively, before anomalous low northern boundary salinity is switched on and maintained for 5 years. Figs. 11, 12 show solutions at 49.25 and 49.75 years corresponding to spring and autumn, respectively, in the final year with anomalous low northern boundary salinity. Increasing the size of c_{ia} leads to a significantly enlarged region of convection with an associated reduction in ice cover (compare Figs. 2, 9). This is consistent with divergence at the ice-edge leading

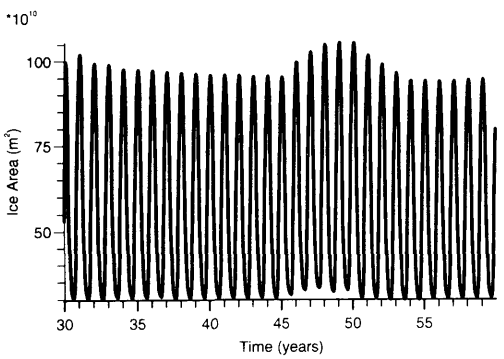

Fig. 14. As in Fig. 13, except for experiment no. 2.

to ice-edge upwelling (Røed and O'Brien, 1983; Häkkinen, 1987) and hence increased entrainment. The introduction of high salinity abyssal water will precondition the ice-edge region for convective overturning which will in turn lead to reduced ice cover. The period of low salinity on the northern boundary significantly reduces the size of the convecting region, particularly in winter. This is shown clearly by comparing time series from 30 to 60 years of ice area for experiment nos. 1, 2 shown in Figs. 13, 14, respectively. There is a clear increase in winter ice area associated with the period of anomalous low salinity northern boundary inflow although this is most evident for experiment no. 2 which has a larger winter convecting region.

6. Conclusions

With the tendency towards ever more complicated coupled ice-ocean models (which require large computer resources) we believe it is useful to develop a simple coupled ice-ocean model which captures the essential physics required for realistic ice modelling on the longer seasonal to interannual time-scales. The successful steady-state coupled ice-ocean model developed by WM has been extended to include time-dependence, simple ice dynamics, variable salinity, horizontal diffusion of heat (already included in a steady-state model by Wood and Mysak (1989)) and salinity, entrainment of abyssal water, a simple convection parameterisation, frazil ice and a prognostic thermodynamic ice concentration equation. The relative simplicity means that this model is a significant step towards the goal of a realistic coupled ice-ocean model which may be inexpensively integrated for long time periods thus rendering it appropriate for climate time-scale problems.

Numerical solutions have been calculated in a meridional channel using parameter values appropriate for the Greenland Sea. Whether convection occurs in the domain (Mysak et al. (1990) suggest that it does in typical winters) is partly controlled by the open boundary salinity distributions. When convection is present the ice forms around the boundary of the convection region. Killworth (1979) points out that typical convectively unstable regions occur on the internal

Rossby radius length scale (typically 10 km in this region). Therefore, a more sophisticated model should include a greater number of much smaller convectively unstable regions. The severe geostrophic constraint implicit in (4.2) and (4.3) together with the hydrostatic balance must be relaxed in a model of the dynamics/thermodynamics of a convecting region. Nevertheless, we believe that our simple parameterisation of vertical mixing provides useful insight into the importance of salinity boundary conditions on ice distribution in coupled ice-ocean models.

The magnitude of the ice-air shear stress also plays an important role in both the steady solutions and the adjustment towards steady-state solutions. For example, the air-ice enhanced shear stress case (experiment no. 2) results in interannual oscillations in the total ice volume as the coupled ice-ocean model adjusts towards a steady state. Obviously, this behaviour could be important in a climate model when the interannual response of a coupled ice-ocean model to interannual forcing fields is of interest.

Time-dependent atmospheric temperature forcing results in large ice-edge movement with the 10%, 50% and 90% ice concentration contours evolving in a similar manner to the observations discussed by Manak and Mysak (1987). In particular the contours are closely spaced in spring with a large poleward meander in the northeast corner due to advection of heat by the cyclonic Greenland Sea gyre. An isolated region of high ice concentration (in excess of 0.9) is obtained in the winter and spring and is frequently observed in the ice concentration field (for example, spring 1972 shown in Fig. 5). In the autumn the isolated region of $A > 0.9$ is completely absent which is also in agreement with observations discussed by Manak and Mysak (1987).

When a time-dependent atmospheric temperature field is combined with a period of fresh northerly inflow many of the features discussed by Mysak et al. (1990) are reproduced. The fresh inflow water is applied and maintained on the northern boundary for 5 years and models the GSA of the 1960s. As the GSA is advected equatorward with the subpolar gyre it produces anomalously large amounts of sea ice.

Perhaps the most serious model deficiency is the use of idealized coastlines. The western boundary is a region of ice convergence and subsequent ice pile-up in the model. However, with a realistic representation of the east Greenland coast there is less likelihood of significant ice convergence occurring. Ice pile-up along the western boundary leads also to a smaller time step requirement (see Section 4.2) and this can be a serious drawback for long integrations of the model. Other improvements to the model will include an interactive atmosphere and an additional ocean layer to improve the vertical resolution.

Acknowledgments

This research is supported by grant GR3/6331 from the UK Natural Environment Research Council. A. J. W. gratefully acknowledges the support of the NATO Collaborative Grant 86/646 which enabled him to visit Professor Mysak at McGill University to discuss this study. We thank Lawrence Mysak for the sea-ice concentration data reproduced in Figs. 4, 5 and Jason Cooper for developing the graphics programs.

Appendix A

Derivation of the quantity S_d

In this Appendix, we derive an expression for the thermodynamic contribution to $\partial d/\partial t$ which we refer to as S_d. The diffusion terms in (3.3) and (3.4) are included for the purpose of numerical solution and hence are relatively small terms. Therefore, throughout this Appendix we set $A_d = A_A = 0$. The heat balance in the time interval $[t_0 - \delta t/2, t_0 + \delta t/2]$ of a column of ice with infinitesimal cross-sectional area $\delta x\, \delta y$ centred at (x, y) is

$$\begin{aligned}
&\rho_i c_i\, \delta t\{\delta y[(u_i A\, d\bar{T}_s)|_{x-\delta x/2} - (u_i A\, d\bar{T}_s)|_{x+\delta x/2}] \\
&\quad + \delta x[(v_i A\, d\bar{T}_s)|_{y-\delta y/2} - (v_i A\, d\bar{T}_s)|_{y+\delta y/2}]\} \\
&\quad + \hat{Q}\, \delta x\, \delta y\, \delta t + \rho_i w_i\, \delta x\, \delta y\, \delta t(c_i T_B + L_w) \\
&\quad = \rho_i c_i\, \delta x\, \delta y[(A\, d\bar{T}_s)|_{t_0-\delta t/2} \\
&\quad - (A\, d\bar{T}_s)|_{t_0+\delta t/2}],
\end{aligned} \tag{A1}$$

where

$$\hat{Q} = A(Q_{wi} - Q_{ia}) + Q_A + Q_{FR}, \tag{A2}$$

$$\bar{T}_S = (T_S + T_B)/2 \qquad w_i = AS_d + dS_A,$$

and we have assumed that water enters and leaves the ice column at temperature T_B. Changes in ice concentration result in a heat flux, Q_A, between the ocean and ice (see (2.4) for an analogous term) defined by

$$Q_A = \rho_i \, dS_A \left[-L_w + c_i \left(\frac{T_s - T_B}{2} \right) \right].$$

Taking the limit $(\delta x, \delta y, \delta t) \to 0$ gives

$$\hat{Q} - \rho_i c_i \nabla \cdot (\boldsymbol{u}_i A \, d\bar{T}_s) + \rho_i w_i (c_i T_B + L_w) = \rho_i c_i \frac{\partial (A \, d\bar{T}_s)}{\partial t}. \tag{A3}$$

We now substitute for $\hat{Q}$ from (A2) into (A3) and employ (3.3) to give (after cancellation of some terms)

$$Q_{wi} - Q_{ia} + \frac{Q_{FR}}{A} = \rho_i c_i S_d \left(\frac{T_s - T_B}{2} \right) - \rho_i L_w S_d + \rho_i c_i d \left(\frac{\partial \bar{T}_s}{\partial t} + \boldsymbol{u}_i \cdot \nabla \bar{T}_s \right). \tag{A4}$$

An expression for $\partial \bar{T}_s / \partial t$ follows from (3.7)

$$\frac{\partial \bar{T}_s}{\partial t} = \hat{\kappa} \left[\frac{\partial d}{\partial t} (T_A - T_s) + \frac{\partial T_A}{\partial t} \right]. \tag{A5}$$

Finally, substituting (A5) into (A4) and employing (3.3) and (3.4) to eliminate $\partial d / \partial t$ gives the required expression, (3.8), for S_d.

Appendix B

Parameter values used in the spin-up experiments

The following parameter values are employed in Subsection 5.1:

$L = 1111.0$ km, $H = 100$ m,

$D = 1.0$ m, $U_0 = 0.05$ m s^{-1},

$T_0 = 2\,^\circ$C, $S_0 = 35$ ppt,

$\rho_0 = 1028$ kg m^{-3}, $\alpha T_0 = 1.44 \times 10^{-2}$,

$\gamma S_0 = 2.73 \times 10^{-2}$,

$c_p = 3987$ J kg^{-1} K^{-1},

$f_0 = 1.37 \times 10^{-4}$ s^{-1},

$\beta = 0.783 \times 10^{-11}$ m^{-1} s^{-1},

$\tau_0 = 0.08$ Nm^{-2}, $T_B = -2.0\,^\circ$C,

$L_w = 335 \times 10^3$ J kg^{-1},

$c_i = 2100.0$ J kg^{-1} K^{-1}, $\rho_i = 0.9\rho_0$,

$\kappa_i = 2.0334$ Wm^{-1} K^{-1}, $S_i = 4.0$ ppt,

$\theta = 45^\circ$, $l = -0.55$, $R_L = 2.75$,

$A_v = 5 \times 10^{-5}$ m^2 s^{-1},

$A_T = A_S = 1000.0$ m^2 s^{-1},

$A_A = 300.0$ m^2 s^{-1}, $A_d = 1500.0$ m^2 s^{-1},

$r = 10^{-6}$ s^{-1}, $A_{max} = 0.98$,

$\kappa_{wa} = 10.0$ Wm^{-2} K^{-1},

$\kappa_{ia} = 8.0$ Wm^{-2} K^{-1}, $q = 0.25$.

References

Batteen, M. L. and Han, Y. J. 1981. On the computational noise of finite-difference schemes used in ocean models. *Tellus 33*, 387–396.

Clarke, R. A., Swift, J. H., Reid, J. L. and Koltermann, K. P. 1990. The formation of Greenland Sea deep water: double diffusion or deep convection? *Deep-Sea Research 376*, 1385–1424.

Crépon, M., Boukthir, M., Barnier, M. and Aikman, F. 1989. Horizontal ocean circulation forced by deep-water formation. *J. Phys. Oceanogr. 19*, 1781–1792.

Darby, M. S. and Mysak, L. A. 1992. A Boolean delay equation model of an interdecadal Arctic climate cycle. *Clim. Dyn.*, in press.

De Szoeke, R. A. 1980. On the effects of horizontal variability of wind stress on the dynamics of the ocean mixed layer. *J. Phys. Oceanogr. 10*, 1439–1454.

Fleming, G. H. and Semtner, A. J. 1991. A numerical study of interannual ocean forcing on Arctic sea ice. *J. Geophys. Res. 96*, 4589–4603.

Gascard, J.C. 1990. Deep convection and deep water formation: progress and new directions. EOS. *Transactions American Geophysical Union 71*, 1837–1839.

Häkkinen, S. 1986. Ice banding as a response of the coupled ice-ocean system to temporally varying winds. *J. Geophys. Res. 91*, 5047–5053.

Häkkinen, S. 1987. A coupled dynamic-thermodynamic

model of an ice-ocean system in the marginal ice zone. *J. Geophys. Res. 92*, 9469–9478.

Häkkinen, S. and Mellor, G. L. 1990. One hundred years of Arctic ice cover variations as simulated by a one-dimensional, ice-ocean model. *J. Geophys. Res. 95*, 15959–15969.

Häkkinen, S., Mellor, G. L. and Kantha, L. H. 1992. Modeling deep convection in the Greenland Sea. *J. Geophys. Res. 97*, 5389–5408.

Haney, R. L. 1974. A numerical study of the response of an idealised ocean to large-scale heat and momentum flux. *J. Phys. Oceanogr. 4*, 145–167.

Hibler, III, W. D. 1979. A dynamic thermodynamic sea-ice model. *J. Phys. Oceanogr. 9*, 815–845.

Hibler, III, W. D. and Bryan, K. 1984. Ocean circulation. Its effects on seasonal sea-ice simulations. *Science 224*, 489–492.

Hibler, III, W. D. and Bryan, K. 1987. A diagnostic ice-ocean model. *J. Phys. Oceanogr. 17*, 987–1015.

Ikeda, M. 1991. Wind-induced mesoscale features in a coupled ice-ocean system. *J. Geophys. Res. 95*, 4623–4630.

Killworth, P.D. 1979. On chimney formations in the ocean. *J. Phys. Oceanogr. 9*, 531–554.

Killworth, P. D. 1983. Deep convection in the world ocean. *Rev. Geophys. Space Phys. 21*, 1–26.

Levitus, S. 1986. Annual cycle of salinity and salt storage in the world ocean. *J. Phys. Oceanogr. 16*, 322–343.

Manak, D. K. and Mysak, L. A. 1987. *Climatic atlas of arctic sea ice extent and anomalies, 1953–1984.* Climate Research Group Report 87-8. Dept. of Meteor. McGill University 214 pp.

Manley, T., Hunkins, K. and Muench, R. 1987. Current regimes across the East Greenland Polar Front at 78°40′ north latitude during summer 1984. *J. Geophys. Res. 92*, 6741–6753.

Marsden, R. F., Mysak, L. A. and Myers, R. A. 1991. Evidence for stability enhancement of sea ice in the Greenland and Labrador Seas. *J. Geophys. Res. 96*, 4783–4789.

McCartney, M. S. and Talley, L. D. 1984. Warm-to-cold water conversion in the northern North Atlantic Ocean. *J. Phys. Oceanogr. 14*, 922–935.

McCreary, J. P. and Yu, Z. 1992. Equatorial dynamics in a $2\frac{1}{2}$-layer model. *Prog. Oceanog. 29*, 61–132.

Mysak, L. A. and Manak, D. K. 1989. Arctic sea-ice extent and anomalies, 1953–1984. *Atmosphere-Ocean 27*, 376–405.

Mysak, L. A., Manak, D. K. and Marsden, R. F. 1990. Sea-ice anomalies observed in the Greenland and Labrador seas during 1901–1984 and their relation to an interdecadal Arctic climate system. *Clim. Dyn. 5*, 111–133.

Ou, H. W. 1991. Some effects of a seamount on oceanic flows. *J. Phys. Oceanogr. 21*, 1835–1845.

Pollard, R. T., Rhines, P. B. and Thompson, R. O. R. Y. 1973. The deepening of the wind-mixed layer. *Geophys. Fluid Dyn. 3*, 381–404.

Riedlinger, S. H. and Warn-Varnas, A. 1990. Predictions and studies with a one-dimensional ice-ocean model. *J. Phys. Oceanogr. 20*, 1545–1562.

Røed, L. P. 1984. A thermodynamic coupled ice-ocean model of the marginal ice zone. *J. Phys. Oceanogr. 14*, 1921–1929.

Røed, L. P. and O'Brien, J. J. 1983. A coupled ice-ocean model of upwelling in the marginal ice zone. *J. Geophys. Res. 88*, 2863–2872.

Semtner, A. J. 1976. A model for the thermodynamic growth of sea ice in numerical investigations of climate. *J. Phys. Oceanogr. 6*, 379–389.

Semtner, A. J. 1987. A Numerical study of sea ice and ocean circulation in the Arctic. *J. Phys. Oceanogr. 17*, 1077–1099.

Stevens, D. P. 1990. On open boundary conditions for three dimensional primitive equation ocean circulation models. *Geophys. Astrophys. Fluid Dyn. 51*, 103–133.

Wadhams, P. 1992. Sea ice thickness distribution in the Greenland Sea and eurasian Basin, May 1987. *J. Geophys. Res. 97*, 5331–5348.

Willmott, A. J. and Darby, M. S. 1990. Nonlinear Rossby waves in a thermodynamic reduced gravity ocean. *Geophys. Astrophys. Fluid Dyn. 54*, 189–227.

Willmott, A. J. and Mysak, L. A. 1989. A simple steady-state ice-ocean model, with application to the Greenland-Norwegian Sea. *J. Phys. Oceanogr. 19*, 501–518.

Wood, R. G. and Mysak, L. A. 1989. A simple ice-ocean model for the Greenland Sea. *J. Phys. Oceanogr. 19*, 1867–1880.

Worthington, L. V. 1970. The Norwegian Sea as a Mediterranean basin. *Deep-Sea Res. 17*, 77–84.